Lab on a Chip

CRITICAL REVIEW

View Article Online
View Journal | View Issue

Cite this: *Lab Chip*, 2026, **26**, 1250

SlipChip: from principle to applications

Yang Luo,[a] Weijie Yuan,[b] Sujin Jung[a] and Feng Shen *[ac]

Received 20th November 2025,
Accepted 27th January 2026

DOI: 10.1039/d5lc01069a

rsc.li/loc

The SlipChip is a versatile microfluidic platform that enables precise control of fluidic connections through the relative sliding of two microstructured plates, without requiring external pumps or valves. SlipChip facilitates fluid aliquoting, mixing, and partitioning *via* a simple sliding operation induced microfluidic reconfiguration. Various designs have been developed and applied to nucleic acid assays, protein crystallization, protein analysis, single-cell analysis, and materials synthesis. Compared with conventional microfluidics, SlipChip offers advantages such as simple fluidic manipulation, on-chip reagent preloading, portability, and cost-effective fabrication in diverse materials (glass, PDMS, plastic, paper). This review summarizes the fluidic principles, device fabrication, and applications of SlipChip, highlighting representative architectures, driving mechanisms, and material considerations. We also address current limitations of SlipChip technology, particularly in terms of assembly precision and dependence on manual operation. Looking forward, advances in materials engineering, device automation, and artificial intelligence are anticipated to enhance assembly reliability and support increasingly autonomous workflows. These developments are poised to significantly broaden the role of SlipChip in systems biology, clinical diagnostics, and personalized medicine. Overall, SlipChip represents a simple, robust, and accessible microfluidic platform suitable for diverse research applications as well as clinical diagnostics.

1 Introduction

Microfluidics enables the manipulation of liquids in small volumes, ranging from microliters to femtoliters. Over the past few decades, various designs and distinct fluid actuation mechanisms have been developed to achieve diverse applications.[1] These include droplet generation by controlling two immiscible fluids,[2] microvalves[3] for opening and closing fluidic paths, electrowetting[4] that modulates surface hydrophobicity *via* applied voltage, centrifugal microfluidics[5] driven by rotational forces, and paper-based microfluidics,[6] among others. Many of these technologies have successfully led to commercial products.

In pursuit of simple, low-cost, instrument-free fluidic manipulation coupled with precise analysis, the SlipChip was introduced. This platform utilizes the relative slipping motion between two closely aligned plates to achieve flexible, and when needed, complex, microfluidic processing.[7] First developed in the Ismagilov Lab for protein crystallization,[8] the SlipChip concept has since evolved significantly. Diverse architectures incorporating various fluidic principles, materials, and fabrication methods have been developed, along with a wide array of applications in nucleic acid analysis,[9] protein studies,[10] bacterial detection,[11] and cellular assays.[12] As a result, the SlipChip has emerged as a powerful tool in biological and clinical research, with considerable potential for translation into commercial microfluidic products.

The SlipChip demonstrates remarkable flexibility in handling sample volumes from milliliters, meeting real-world analytical requirements, down to nanoliters and picoliters for digital nucleic acid[13] and cell analysis, and even femtoliters for digital immunoassays. It also supports parallel multistep processing across large arrays, enabling multi-step assays with ease. In addition to droplet merging, the platform allows droplet splitting for various analytical purposes. Integration with functional components such as magnetic beads and electrodes further extends its utility. Moreover, the SlipChip can be applied to generate microparticles with varied shapes and compositions.

In this review, we systematically summarize the development of SlipChip technology with respect to fluidic actuation mechanisms, materials and fabrication methods, and applications. We compare different designs and interpret their underlying principles. Finally, we discuss current challenges and future opportunities, highlighting how advances in materials, automation, and artificial intelligence

[a] *School of Biomedical Engineering, Shanghai Jiao Tong University, Shanghai 200030, China. E-mail: feng.shen@sjtu.edu.cn*
[b] *State Key Laboratory for Diagnosis and Treatment of Severe Zoonotic Infectious Diseases, Key Laboratory for Zoonosis Research of the Ministry of Education, Institute of Zoonosis, and College of Veterinary Medicine, Jilin University, Changchun 130062, China*
[c] *Zhengzhou Industrial Technology Research Institute of Shanghai Jiao Tong University, Zhengzhou, 450016 China*

could further extend the potential of SlipChip in systems biology, diagnostics, and personalized medicine.

This layout is represented in Fig. 1.

2 Fluidic operation principles of SlipChip

2.1 Fundamental concept: slip-induced reconfiguration

The fundamental principle of the SlipChip lies in its ability to precisely manipulate microscale fluids through controlled sliding. A typical SlipChip consists of plates patterned with microstructures such as wells and microchannels. The relative sliding of these plates alters their alignment, enabling the connection or disconnection of fluidic paths, as well as the merging and splitting of droplets. The surfaces of both plates are silanized to be hydrophobic and a lubricating oil is placed in-between the two plates during device assembly to prevent liquid evaporation and eliminate undesirable air–water interfaces that may interfere with certain applications. When microwells or chambers are aligned to form a continuous fluidic path, a unidirectional pressure greater than capillary pressure but below the maximum sealing pressure is applied to introduce fluid into the microstructures,[14] thereby preventing aqueous solutions from leaking into the interstitial gap between the plates. When a shallow aqueous channel comes into contact with a deeper oil-filled channel, the aqueous phase spontaneously flows into the deeper channel due to capillary-driven forces.[15] As a result, various solutions and complex biological media can displace the oil phase while being introduced into the chip and filling the deeper microstructures due to the hydrophobicity of the SlipChip and the geometric constraints of its design, whereas the displaced oil escapes through connected channels or micron-scale gaps between the plates.[16] Once loading is completed, subsequent sliding of the plates disconnects the fluidic paths, isolating the microchambers and forming individual reaction compartments.

2.2 Various types of SlipChip design

Digital SlipChip. Digital analysis often requires microfluidic chips to generate large numbers of droplets for parallel reactions. Based on the mentioned operation process, three digital SlipChip platforms have been developed that are capable of producing thousands of uniformly sized droplets specifically for this purpose. The original SlipChip design features overlapping wells with complementary geometries. When two plates are assembled, the wells on the top and bottom plates partially overlap, forming continuous fluidic pathways in a "hand-in-hand" configuration.[8] After loading aqueous reagents into the device using a pipette, the plates are slid into an isolated position, disconnecting the fluidic pathways and aligning microchambers with their corresponding "receiving" wells (Fig. 2A). The oil phase between the plates acts as a lubricant and facilitates droplet formation. This method does not require any external fluidic control system, providing a valuable tool for applications in

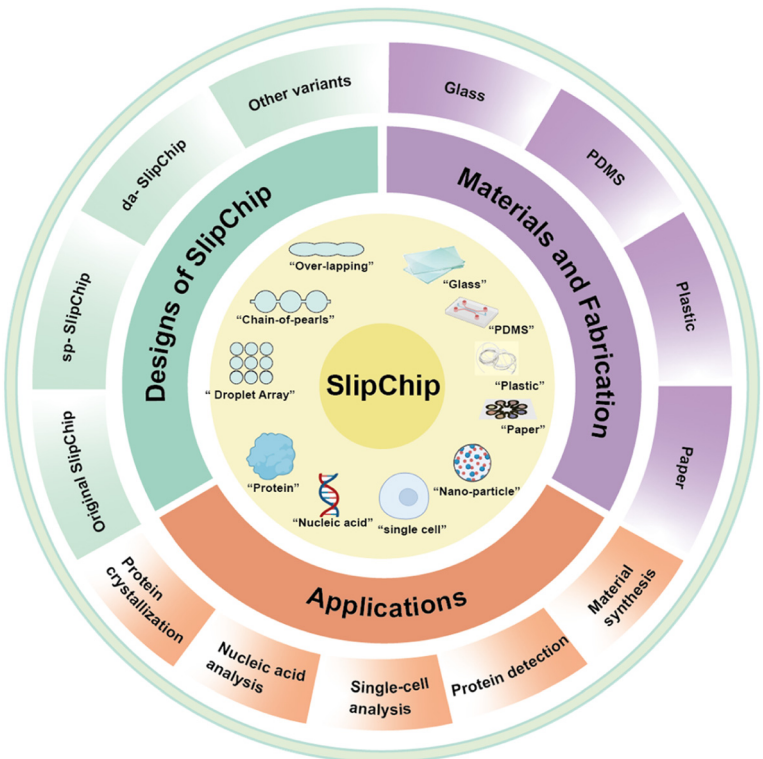

Fig. 1 Schematic overview of the SlipChip.

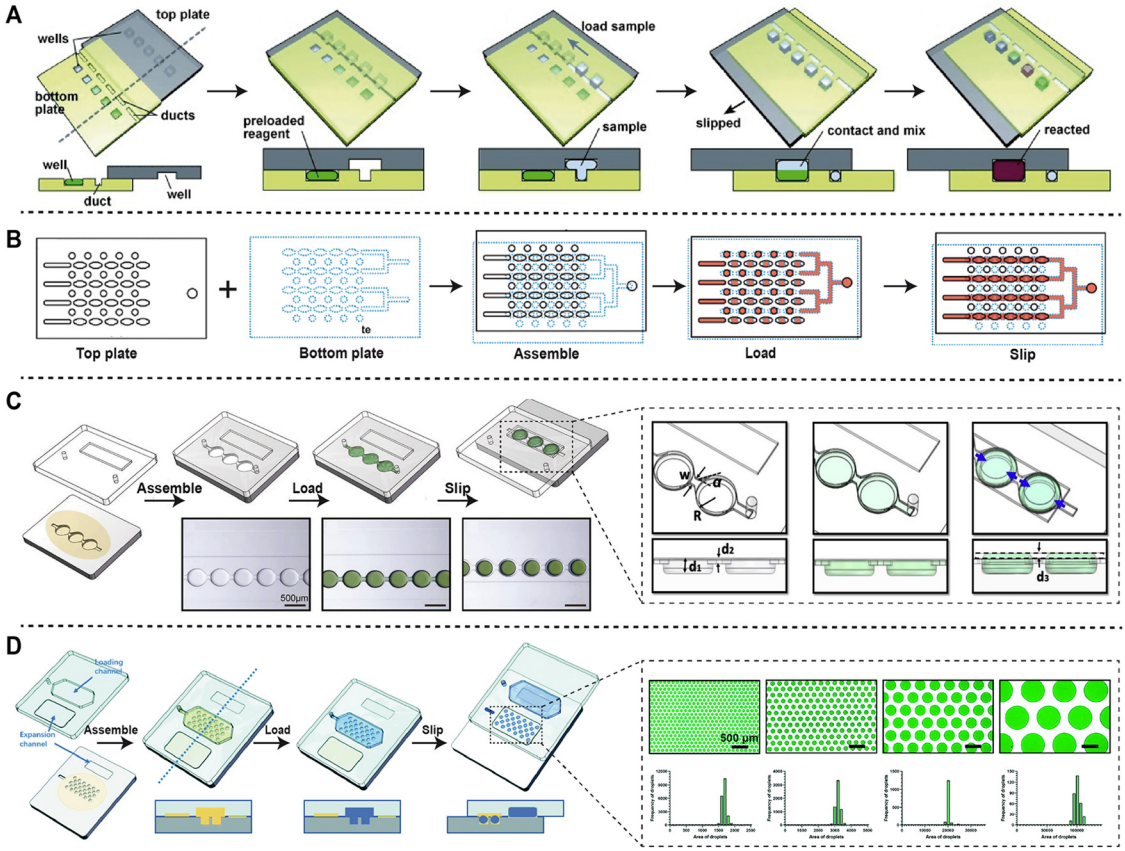

Fig. 2 Three digital SlipChip platforms used to generate large numbers of droplets. (A) Schematic of original SlipChip. Reproduced with permission from ref. 8. Copyright 2009, Royal Society of Chemistry. (B) Schematic of original digital SlipChip. Reproduced with permission from ref. 17. Copyright 2010, Royal Society of Chemistry. (C) Schematic of self-partitioning digital SlipChip. Reproduced with permission from ref. 18. Copyright 2020, Elsevier. (D) Schematic of droplet-array digital SlipChip. Reproduced with permission from ref. 19. Copyright 2021, Royal Society of Chemistry.

resource-limited settings. Building on this design, Shen *et al.* developed the first digital SlipChip, capable of generating 1280 droplets of 2.6 nL each with a single slide[17] (Fig. 2B). To further reduce alignment requirements, the self-partitioning SlipChip (sp-SlipChip) was developed. Unlike the original SlipChip, the sp-SlipChip introduces fluid through independent "chain-of-pearls" microchannels. A sliding step subsequently overlaps the chain-of-pearls channels with extended channels on the opposing plate. Driven by surface tension differences between the microwell and "neck" of each pearl, the continuous liquid breaks at each "neck" and then expands to form discrete droplets. This slip-induced self-partitioning process is regulated by the physical geometry and surface properties of the "chain-of-pearls" channels, making the process highly robust and capable of generating large numbers of droplets reproducibly. Compared with original SlipChip, this design greatly reduces operational complexity. Based on this principle, Yu *et al.* developed a self-partitioning SlipChip capable of generating 2240 droplets of 4.5 nL each in a single operation[18] (Fig. 2C). To further increase the droplet number, the droplet-array SlipChip (da-SlipChip) was developed, enabling droplet volumes to be reduced to the femtoliter range. Different from the previous two designs, the da-SlipChip consists of a dense array of nanoliter- to femtoliter-scale microwells on one plate and a wide loading channel on the other plate that covers the entire microwell region. During the loading step, the fluidic channel on the top plate is fully aligned with the microwell array on the bottom plate. The solution is then introduced from the inlet, and due to the adoption of a dead-end filling structure,[14] the liquid fills both the loading channel and all microwells under the combined effects of surface tension and applied pressure. A subsequent sliding step misaligns the two plates, efficiently partitioning the reaction mixture into an array of discrete droplets (Fig. 2D). Using this design, Lyu *et al.* achieved the high-throughput generation of up to 21 696 droplets of 250 pL in a single reaction,[19] and further demonstrated that by integrating precise dry-etching techniques, millions of microwells as small as 50 fL could be fabricated (Table 1).[20]

Parallel droplet manipulation SlipChip. Complex biochemical processes, such as single-cell analysis, pose significant challenges for microfluidic platforms, which must be capable of performing precise, multistep, and parallel fluidic operations. The physical overlap between the microwells on the two plates of a SlipChip offers a simple

Table 1 Comparison of representative SlipChip designs across key metrics

SlipChip design	Typical droplet volume	Number of partitions	Representative applications
Digital SlipChip	~0.00005–625 nL	~10^2–10^6 droplets	Digital nucleic acid analysis;[17–19,50–54,57,61,62] digital immunoassay;[20,75,76] single-cell phenotypic analysis;[87] digital phage quantification[90]
Parallel droplet manipulation SlipChip	~0.2–2000 nL	~10^2–10^4 droplets	Digital nucleic acid analysis;[21,23] RNA sequencing;[22] immunoassay;[69] single-cell metabolic analysis[92]
Free-interface diffusion (FID) SlipChip	~10–1000 nL	~10^2–10^3 droplets	Protein crystallization;[25] antimicrobial susceptibility testing[27]
Preloaded SlipChip	~20–1000 nL	~10^2–10^3 droplets	Protein crystallization;[8] multiplex nucleic acid analysis;[29] antimicrobial susceptibility testing[30]
Serial dilution SlipChip	~1–100 nL	~10^2–10^3 droplets	Digital nucleic acid analysis;[31] antimicrobial susceptibility testing;[32] enzyme inhibitor screening[33]
Nano-matrix SlipChip	~10–100 nL	~10^2–10^3 droplets	Drug screening[34]

and effective method for controlled droplet fusion. In the original SlipChip, two separate loading channels were designed on each side of the device to generate two distinct droplet arrays, which could subsequently be aligned through sliding, allowing paired droplets to merge (Fig. 3A).

Using this strategy, Shen *et al.* successfully separated the loading of RPA reagents and magnesium ion initiators, thereby preventing pre-amplification and improving the accuracy of digital RPA quantification.[21] To enable more complex multistep manipulations of droplets, Zhukov *et al.* developed a capillary (Laplace) pressure-driven multistep SlipChip.[22] In this design, a series of deeper mixing wells are patterned on one plate, while corresponding carrier wells are fabricated on the other. Sliding the two plates brings the carrier wells into alignment with the mixing wells. Owing to the capillary pressure imbalance arising from differences in feature dimensions at the front and back of the droplet, the regent droplets in the carrier wells are transferred into the deeper mixing wells (Fig. 3B). By carefully engineering the microscale geometries to control this capillary pressure

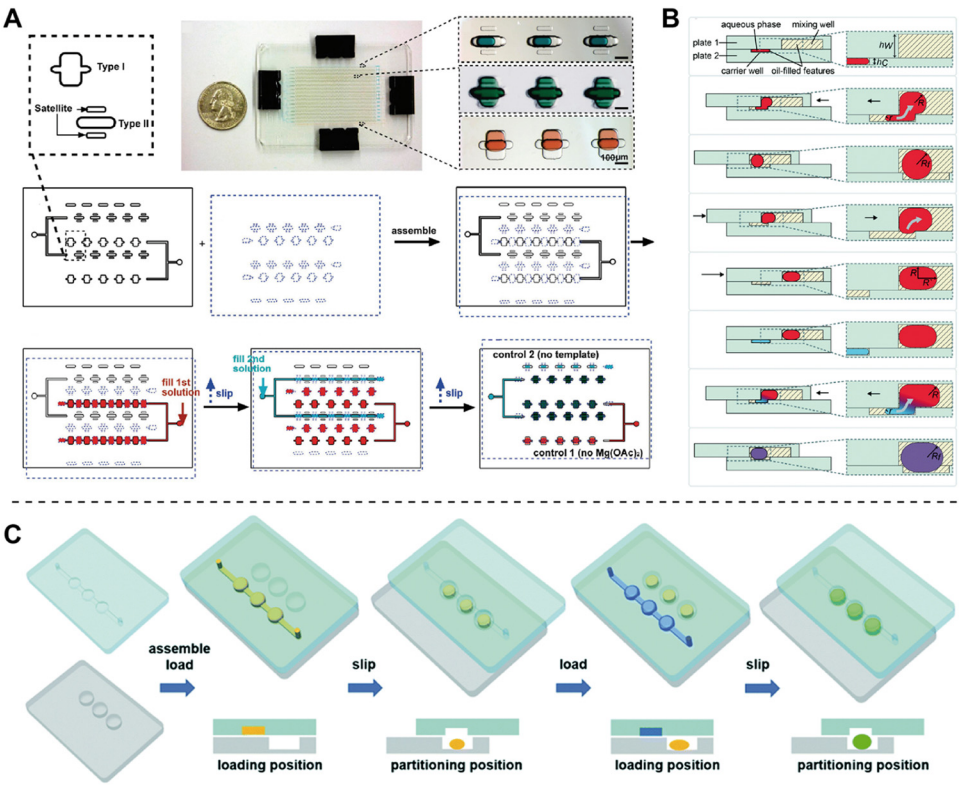

Fig. 3 Schematic drawings of SlipChip designed for parallel droplet manipulation. (A) Schematic drawing of the original SlipChip with two separate loading channels. Reproduced with permission from ref. 21. Copyright 2011, American Chemical Society. (B) Schematic drawing of the capillary (Laplace) pressure-driven multistep SlipChip. Reproduced with permission from ref. 22. Copyright 2019, Royal Society of Chemistry. (C) Schematic drawing of parallel multistep digital analysis SlipChip (PAMDA). Reproduced with permission from ref. 23. Copyright 2022, Royal Society of Chemistry.

imbalance, the device enables parallel droplet merging through sequential sliding steps. Using this approach, multistep reactions such as RNA barcoding for multiplexed RNA sequencing (RNA-Seq) were successfully demonstrated on the SlipChip. Similarly, to further increase the throughput of multistep droplet manipulation, Yu *et al.* combined this design with the self-partitioning SlipChip to develop a parallel multistep digital analysis SlipChip (PAMDA) (Fig. 3C), which enables the simultaneous generation and merging of 2400 droplets.[23] This platform successfully combined loop-mediated isothermal amplification (LAMP) with clustered regularly interspaced short palindromic repeats (CRISPR)- or argonaute (Ago)-based detection,[24] enabling rapid and fully digital nucleic acid quantification through a two-step reaction workflow.

Free-interface diffusion (FID) SlipChip. Microfluidic systems capable of generating gradient concentration conditions provide sealed microenvironments with small reaction volumes, enabling high-throughput biological and chemical screening. The free-interface diffusion (FID) method offers a convenient and efficient approach for establishing concentration gradients and temporal profiles within microfluidic devices. By controlling the connection and disconnection of liquids within microchannels, the SlipChip can generate a series of concentration gradients within the device through molecular diffusion. Li *et al.* integrated FID techniques into a composite SlipChip[25] (Fig. 4A).

When the SlipChip was "slipped" to connect the protein and precipitant wells, different screening conditions were achieved by gradually increasing the diffusion distance between the two wells or by changing the microchamber volumes. Using this approach, 176 protein crystallization experiments could be performed simultaneously within a single device. In addition, by allowing multiple test sets to be performed in parallel on the chip, this design provides a valuable platform for testing multiple proteins and conducting high-throughput screening assays. This diffusion-based approach also can be applied to create concentration gradients for a variety of studies, such as for diverse biological applications, including studies of chemotaxis and cellular responses.[26] Liu *et al.* further developed a gradient droplet SlipChip (gd-SlipChip)[27] (Fig. 4B), which combines the principles of the self-partitioning SlipChip and the multistep SlipChip. In this design, a "chain-of-pearls" microchannel first enables diffusion between adjacent compartments to establish a series of antibiotic concentration gradients. These gradient droplets are then transferred into larger mixing wells, while the chain-of-pearls channels can serve as loading channel for bacterial suspensions. Subsequent sliding merges the bacterial suspension with the gradient droplets, enabling phenotypic antimicrobial susceptibility testing (AST) in a compact and parallelized format.

Preloaded SlipChip. Multiplexed experiments are common in both biological and chemical research. The fixed

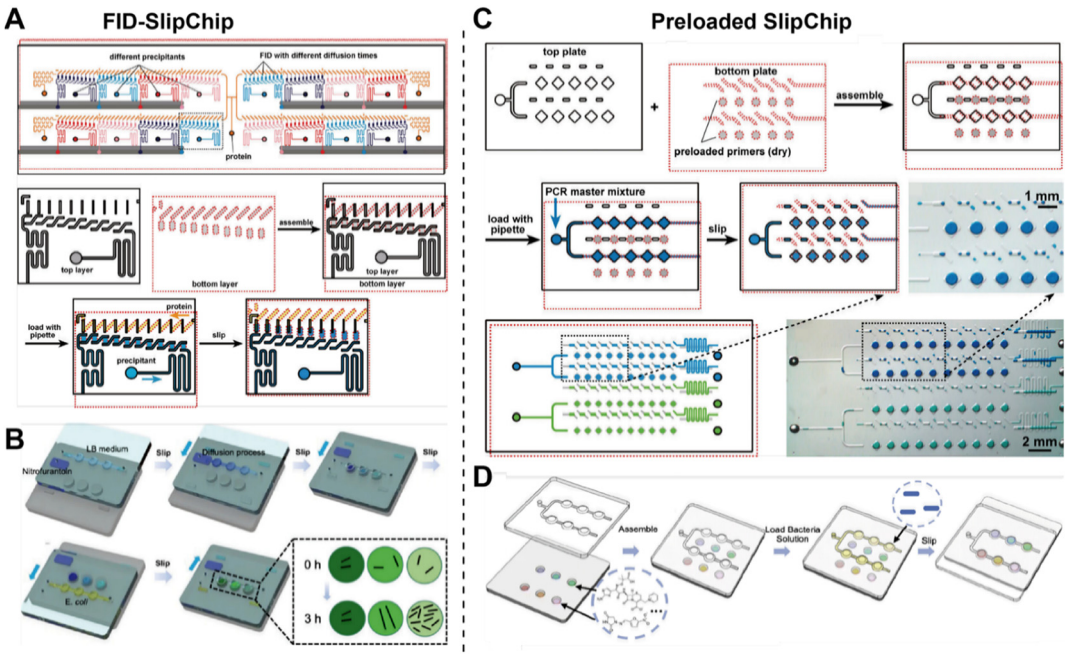

Fig. 4 Schematic illustration of SlipChip designs that enable free-interface diffusion and allow reagent preloading in the device. (A) Schematic drawing of the composite SlipChip integrated FID techniques. Reproduced with permission from ref. 25. Copyright 2009, American Chemical Society. (B) Schematic drawing of the gradient droplet SlipChip (gd-SlipChip). Reproduced with permission from ref. 27. Copyright 2022, American Chemical Society. (C) Schematic drawing of the primer-preloaded SlipChip. Reproduced with permission from ref. 29. Copyright 2010, American Chemical Society. (D) Schematic drawing of the combinatorial screening SlipChip (cs-SlipChip) that allow preloading different antibiotics. Reproduced with permission from ref. 30. Copyright 2022, Royal Society of Chemistry.

partitioning positions of the SlipChip provide a powerful platform for high-throughput biochemical reactions. Biological samples and reagents have been shown to remain stable on the SlipChip after drying and can be rehydrated for subsequent laboratory analyses.[28] Taking advantage of this feature, reagents can be preloaded into the microstructures of the SlipChip and preserved through freezing or chemical matrix drying. The reagents can be subsequently distributed for target screening, greatly simplifying experimental workflows and enabling multiplexed experiments. Shen *et al.* developed a preloaded SlipChip for nanoliter-scale multiplex PCR by pre-depositing dried primer reagents into microwells (Fig. 4C). With a single sliding step, the device could screen up to 384 distinct primer pairs, significantly improving diagnostic efficiency.[29]

In addition, by preloading different dried antibiotics into a sp-SlipChip and rehydrating them in parallel, a combinatorial screening SlipChip (cs-SlipChip) was developed for rapid phenotypic antimicrobial susceptibility testing (Fig. 4D). This device enabled 192 parallel phenotypic ASTs within 3 hours, providing a compact and efficient solution for antibiotic screening.[30]

Serial dilution SlipChip. Serial dilution is a widely used technique for establishing screening conditions across a broad dynamic range, with applications in biological research, reaction optimization, and drug discovery. Traditionally, generating a series of serial dilutions requires labor-intensive manual pipetting or robotic liquid-handling systems. Multistep SlipChip provides a promising miniaturized alternative for creating nanoliter-scale serial dilutions with high precision. By carefully designing pairs of interconnected "parent" and "daughter" wells with predefined volume ratios, the serial dilution SlipChip (sd-SlipChip) (Fig. 5A) enables controlled transfer of liquid between wells during sequential sliding steps. Each sliding motion establishes a temporary fluidic connection that allows a portion of the solution from the parent well to mix with dilution buffer in the daughter well, thereby producing a new dilution.[31] Repeating this process across multiple well pairs can yield a series of accurately defined concentration gradients directly on the chip. Yu *et al.* used this device to achieve digital nucleic acid quantification by serial dilution of target molecules, with a theoretical dynamic range across seven orders of magnitude within 600 microwells. Beyond nucleic acid analysis, this approach is also suitable for other bioassays that require continuous dilution gradients. Based on this concept, Wang *et al.* developed a nano-dilution SlipChip (nd-SlipChip) (Fig. 5B) that produces antibiotic concentration gradients. This design enables rapid and accurate assessment of bacterial susceptibility, providing a fast and precise platform for antimicrobial resistance testing.[32] In addition, the same principle can be extended to generate drug concentration gradients for enzyme inhibitor screening[33] (Fig. 5C).

Nano-matrix SlipChip. In addition, to further increase testing throughput, a nanoliter matrix SlipChip (nm-SlipChip) (Fig. 5D) was developed. In this device, both plates contain partial microfluidic structures, with spindle-shaped

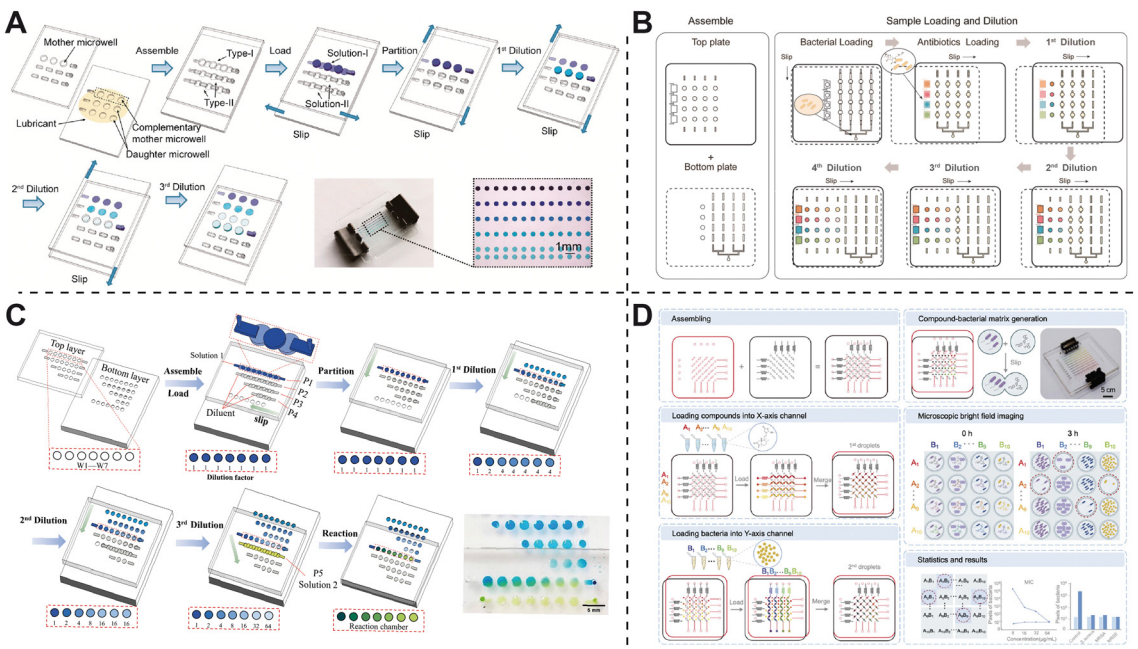

Fig. 5 Schematic illustration of SlipChip designs that enable on-chip serial dilution and allow droplet-matrix mixing. (A) Schematic drawing of the serial dilution SlipChip (sd-SlipChip). Reproduced with permission from ref. 31. Copyright 2019, American Chemical Society. (B) Schematic drawing of the nano-dilution SlipChip (nd-SlipChip). Reproduced with permission from ref. 32. Copyright 2025, Elsevier. (C) Serial dilution SlipChip for enzyme inhibitor screening. Reproduced with permission from ref. 33. Copyright 2023, MDPI, under CC BY license. (D) Schematic drawing of the nanoliter matrix SlipChip (nm-SlipChip). Reproduced with permission from ref. 34. Copyright 2025, Wiley-VCH GmbH.

microwells arranged orthogonally. Different alignments create fluidic channels along the *X* and *Y* axes, allowing compound droplet arrays to be formed first along the *X* axis, followed by antibiotic droplet arrays along the *Y* axis.

Orthogonal mixing of bacterial samples with these droplets generates highly multiplexed combinatorial matrices, which have been successfully applied for high-throughput screening of antibiotic candidates derived from natural products.[34] By incorporating a microfluidic dilution network into both plates, the similar design enables the generation of two orthogonal and independent concentration gradients across different planes. Subsequent sliding of the chip allows the mixing of samples and reagents at varying concentrations, facilitating multiplexed reactions.[35] Overall, the design of SlipChip continues to evolve toward increasing diversity, enabling their adaptation to a broad range of analytical and biological applications.

3 Materials and fabrication methods

SlipChip can be fabricated from a wide variety of materials, allowing them to be adapted for different application requirements. The materials and fabrication methods currently used for SlipChip construction primarily include the following categories (Table 2).

Glass

Glass, including soda-lime glass and quartz, is one of the most commonly used substrates for SlipChip fabrication. Conventional SlipChip is typically made from glass plates patterned with microstructures through dry or wet etching processes. Its rigidity, smoothness, and amenability to diverse surface chemistries further make glass an excellent substrate for precise microfabrication and reliable microfluidic operation. Due to its chemical inertness, optical transparency, and stable surface properties (especially after hydrophobic surface treatment), glass is highly suitable for a wide range of biochemical reactions. In addition, its excellent resistance to organic solvents and high temperatures makes it ideal for analytical applications such as PCR and immunoassays. However, glass fabrication usually requires cleanroom-based processes, including photomask design and etching, which are time-consuming and expensive, thereby limiting scalability and large-scale production.

PDMS

Polydimethylsiloxane (PDMS) is another widely used material for microfluidic device fabrication. Owing to its excellent biocompatibility, gas permeability, tunable elasticity, and optical transparency, PDMS has been extensively employed in applications such as cell culture and organ-on-a-chip systems.[36] SlipChip can also be fabricated from PDMS using soft lithography techniques. Chang *et al.* first developed a PDMS-based SlipChip[37] and successfully performed mammalian cell co-culture and cytokine assays on the device, demonstrating its great potential for *in vitro* cell biology research. Inaam *et al.* further optimized the viscosity of silicone oil and the curing conditions of PDMS to improve the sealing, slipping performance, and biocompatibility of PDMS SlipChip.[38]

Despite its low cost and well-established fabrication protocols, large-scale production remains challenging due to the relatively intricate manufacturing process. Moreover, PDMS exhibits inherent hydrophobicity due to the presence of surface $-CH_3$ groups and tends to absorb small hydrophobic molecules and proteins, which can be detrimental in certain analytical or biochemical applications.[39]

Plastic

To enhance the mass manufacturing capacity of SlipChip, rigid plastics such as poly(methyl methacrylate) (PMMA) and polycarbonate (PC) have been considered particularly attractive materials. These thermoplastics can be produced on a large scale at low per-unit cost using mass-production techniques such as injection molding or CNC machining. PMMA-based micromachining methods have already been employed for SlipChip fabrication,[40] enabling the rapid creation of microstructures on the chip surface. Similarly, a microfluidic sample preparation platform termed "Slipdisc", based on the SlipChip principle, utilized PC material that can be injection molded,[41] making it highly suitable for batch manufacturing. In addition, polymer-based materials such as

Table 2 Summary of common materials used in SlipChip fabrication, highlighting their fabrication approaches, advantages, and limitations for different analytical contexts

Material	Advantages	Limitations	Typical fabrication method	Representative applications
Glass	High precision; excellent optical clarity; solvent and temperature resistant	Expensive; cleanroom processes required; limited scalability	Photolithography, wet/dry etching	Protein crystallization;[8,25,66] nucleic acid analysis;[17–19,50–54] immunoassays[20,69,70,74]
PDMS	Low cost; biocompatibility; gas permeability	Absorbs hydrophobic molecules; poor for mass production	Soft lithography, casting in SU-8 molds	Cell culture;[37] organ-on-a-chip; nucleic acid analysis[46]
Plastic	Mass-producible; low cost; suitable for disposable use	Mold precision critical; bonding or warping issues, surface smoothness	Injection molding, hot embossing, 3D printing	Point-of-care diagnostics;[63–65] disposable assays
Paper	Ultra-low cost; pump-free capillary flow; simple tools	Limited solvent compatibility; poor optical clarity	Wax printing, lamination	Point-of-care diagnostics[71,72]

resin have been used to fabricate SlipChip *via* digital light processing (DLP) 3D printing,[42] and multi-material 3D printing combining rigid and elastic components within a single part,[43] offers convenient customization for functional SlipChip devices. Establishing design principles for 3D-printed SlipChip will further enhance the capability for rapid prototyping and medium-scale production. While these materials and methods can greatly accelerate fabrication, they may still encounter limitations in precision and surface smoothness, which in turn can constrain the reliable formation of very fine microstructures. Moreover, injection molding processes are inherently constrained by mold design limitations.

Paper

Furthermore, to further reduce fabrication costs, SlipChip technology can also be integrated with paper-based microfluidics. Using wax-printing techniques, microfluidic patterns can be printed onto chromatography paper and then attached to a rigid substrate, leading to the development of a paper-based SlipChip (SlipPAD).[44] This type of SlipChip can be fabricated rapidly and at very low cost, at less than $1 USD per device, requiring only a $600 wax printer and a hot plate. In addition, functionalization of the paper-based SlipChip surface with nanoparticles enables efficient signal readout such as colorimetric detection, making it particularly suitable for point-of-care testing (POCT).[45] As with many paper-based technologies, these advantages are accompanied by certain practical constraints. Detection sensitivity and limits are generally lower, and chemical compatibility can be restricted—for example, such devices are not suitable for use with organic solvents that may dissolve the wax patterns.

4 Applications of SlipChip

SlipChip has been broadly applied in chemical and bioanalytical research. The main application areas include nucleic acid analysis, protein crystallization, protein assays, cell and bacterial assays, and materials synthesis.

4.1 Nucleic acid analysis

Multiplex nucleic acid analysis. Multiplex nucleic acid analysis (NAA) allows the simultaneous detection of multiple target nucleic acids, making it highly appealing for life science research and clinical diagnostics. Multiplex NAA can be performed by physically separating each target of interest into distinct regions. Through spatially encoded reagent preloading, the SlipChip enables 384 parallel nanoliter PCR reactions without external fluidic control[29] (Fig. 6A).

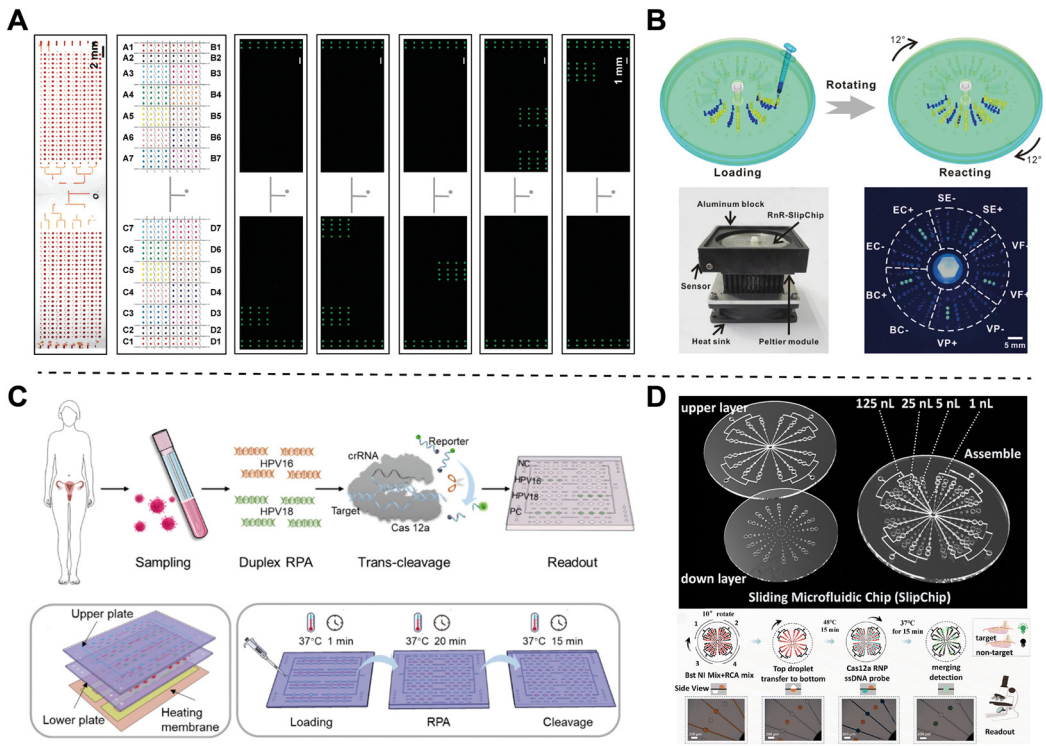

Fig. 6 SlipChip for multiplex nucleic acid analysis. (A) Nanoliter multiplex PCR arrays on a preloading SlipChip. Reproduced with permission from ref. 29. Copyright 2010, American Chemical Society. (B) A rotational SlipChip enabling simultaneous LAMP analysis of five common bacterial pathogens. Reproduced with permission from ref. 46. Copyright 2016, Elsevier. (C) Simultaneous detection of HPV16 and HPV18 by RPA and CRISPR assays. Reproduced with permission from ref. 47. Copyright 2024, American Chemical Society. (D) An RCA-CRISPR/Cas12a assay on a multivolume SlipChip for quantification of circRNA and miRNA. Reproduced with permission from ref. 48. Copyright 2025, Royal Society of Chemistry.

Moreover, by performing multiple compartmentalized reactions in parallel, a rotational SlipChip has been used to accomplish one-step multiplex detection, enabling simultaneous LAMP analysis of five common gastrointestinal bacterial pathogens[46] (Fig. 6B). To further enhance the specificity of isothermal amplification, CRISPR/Cas systems have also been incorporated into SlipChip platforms through multistep fluid manipulation. Zhao *et al.* integrated RPA and CRISPR assays into a heating-membrane-assisted SlipChip device, enabling simultaneous detection of HPV16 and HPV18 (ref. 47) (Fig. 6C). To improve sensitivity, Tian *et al.* developed an RCA-CRISPR/Cas12a assay on a multivolume SlipChip, achieving ultrafast, single-copy quantification of circRNA and miRNA in ovarian cancer samples. This platform reached detection limits of 0.125 copies per μL for circRNA and 0.326 copies per μL for miRNA, covering a five-log dynamic range (10^{-1}–10^{3} copies per μL) within only 35 minutes[48] (Fig. 6D).

Digital nucleic acid analysis. Digital NAA based on SlipChip enables absolute quantification of nucleic acids by partitioning a sample into a large number of uniform nanoliter or picoliter compartments. Various SlipChip designs employing different fluidic control principles have been developed to generate droplet arrays for digital nucleic acid quantification. One of the most established formats is digital PCR (dPCR), which relies on thermal cycling for amplification. The original SlipChip design produced 1280 nanoliter droplets, achieving the first demonstration of digital PCR and enabling absolute quantification of *Staphylococcus aureus* genomic DNA[17] (Fig. 7A). In single-

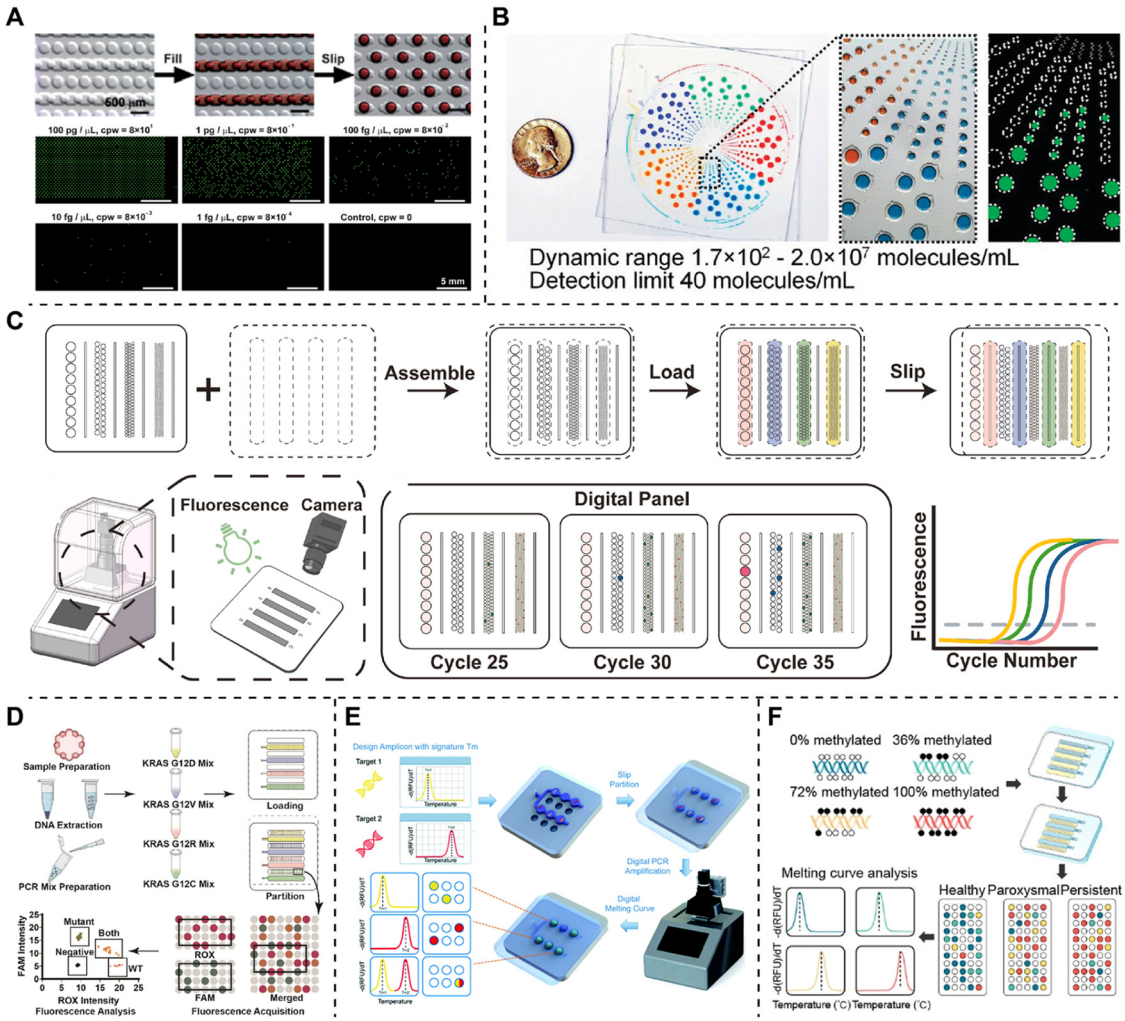

Fig. 7 SlipChip for digital PCR. (A) The original SlipChip for digital PCR quantification of an *S. aureus* gene. Reproduced with permission from ref. 17. Copyright 2010, Royal Society of Chemistry. (B) A multivolume SlipChip device for simultaneous quantification of HIV and HCV viral loads by digital RT-PCR. Reproduced with permission from ref. 50. Copyright 2011, American Chemical Society. (C) A real-time digital PCR system with a multivolume da-SlipChip to study the kinetics of digital PCR. Reproduced with permission from ref. 51. Copyright 2024, Elsevier. (D) Multicolor hydrolysis probes integrated into the SlipChip for simultaneous KRAS mutation quantification. Reproduced with permission from ref. 52. Copyright 2022, American Chemical Society. (E) Multiplex detection of five pathogenic microorganisms using sp-SlipChip based on digital MCA. Reproduced with permission from ref. 53. Copyright 2022, Royal Society of Chemistry. (F) A digital MCA method using a da-SlipChip to assess methylation heterogeneity. Reproduced with permission from ref. 54. Copyright 2023, American Chemical Society.

volume digital PCR, the upper limit of quantification (ULQ) is mainly dictated by the volume of individual wells, whereas the lower detection limit (LDL) depends on the total reaction volume. As a result, achieving a broad dynamic range would typically require tens of thousands to millions of partitions.[49]

To address the issue of dynamic range without relying on a large number of droplets, Shen *et al.* developed a multi-volume SlipChip for digital RT-PCR (Fig. 7B), which incorporated 160 wells each of four different volumes (125 nL, 25 nL, 5 nL, and 1 nL). This design achieved a theoretical dynamic range from 5.2×10^2 to 4.0×10^6 molecules per mL without requiring a large number of droplets, and successfully quantified HIV and HCV RNA.[50] Building upon this concept, Luo *et al.* developed an integrated fluorescence monitoring system to investigate single-molecule amplification kinetics across multiple droplet volumes (Fig. 7C), experimentally validating the "confinement effect" in digital PCR. A digital-analog quantification strategy was

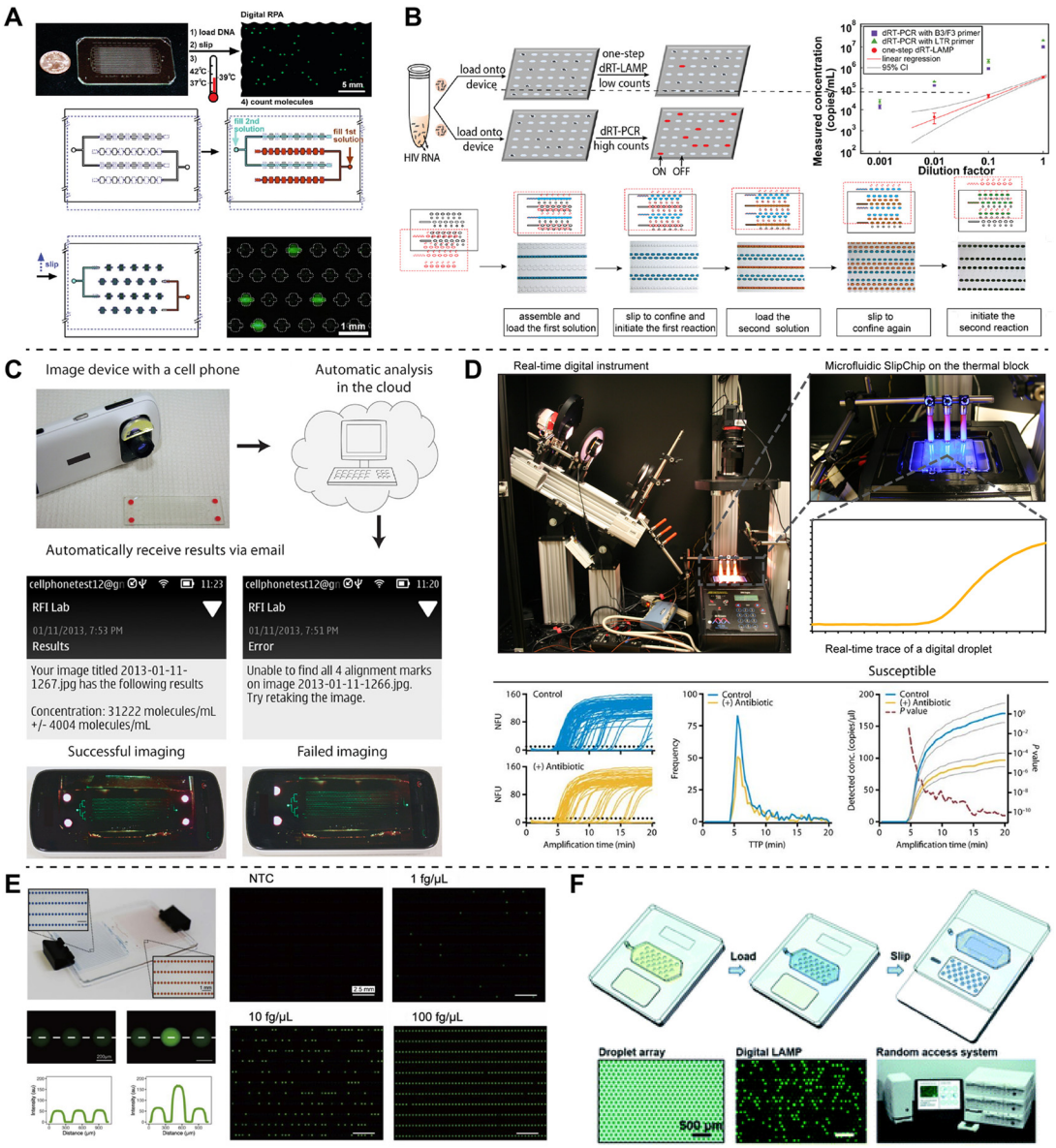

Fig. 8 SlipChip for digital isothermal nucleic acid amplification. (A) The two-step SlipChip for digital RPA. Reproduced with permission from ref. 21. Copyright 2011, American Chemical Society. (B) One-step RT-LAMP has lower efficiency and a SlipChip device for two-step digital RT-LAMP. Reproduced with permission from ref. 57. Copyright 2013, American Chemical Society. (C) The smartphone imaging workflow used to count molecules *via* digital LAMP with a SlipChip. Reproduced with permission from ref. 58. Copyright 2013, American Chemical Society. (D) An instrument for real-time digital LAMP on SlipChip devices, applied for digital dAST of clinical UTI urine samples. Reproduced with permission from ref. 59. Copyright 2016, *PLoS One*; reproduced with permission from ref. 60. Copyright 2017, American Association for the Advancement of Science (AAAS). (E) The sp-SlipChip for digital LAMP quantification of HPV detection. Reproduced with permission from ref. 18. Copyright 2020, Elsevier. (F) The da-SlipChip for digital LAMP quantification of SARS-CoV-2 nucleic acids. Reproduced with permission from ref. 19. Copyright 2021, Royal Society of Chemistry.

further proposed to extend the dynamic range of digital PCR by integrating real-time quantification, achieving up to seven orders of magnitude in dynamic range.[51] To further extend the multiplex capability, multicolor hydrolysis probes have been integrated into the SlipChip platform, enabling simultaneous quantification of KRAS 12C, D, R, and V mutations as well as the wild-type gene[52] (Fig. 7D).

Moreover, taking advantage of the fixed droplet positions that allow real-time monitoring, integration of an on-chip real-time fluorescence detection system has enabled multiplex molecular analysis through digital melting curves analysis (MCA) of five common pathogenic microorganisms[53] (Fig. 7E) and differential DNA methylation states terms of methylation level and methylation density[54] (Fig. 7F). These advancements have greatly expanded the multiplexing potential of the SlipChip platform.

Beyond implementing digital PCR on the SlipChip, the platform has been further extended to isothermal amplification methods, eliminating the need for thermal cycling. However, achieving accurate quantification with digital isothermal nucleic acid amplification presents several challenges. Firstly, unlike "hot-start" PCR polymerases that are activated at high temperatures, recombinase polymerase amplification (RPA) can proceed at room temperature with a slow amplification rate.[55] To address this, a two-step SlipChip design with parallel droplet manipulation was employed to eliminate pre-amplification "background" in digital RPA by physically separating the initiator and the reaction mixture[21] (Fig. 8A). Secondly, differences in the "digital amplification efficiency" between LAMP and PCR may lead to slightly lower digital counts than expected when performing one-step dRT-LAMP on a SlipChip.[56] By taking advantage of the SlipChip's capability for two-step reagent loading, a two-step RT-LAMP method was developed. In the RT step, only the BIP primer is added, followed by the introduction of RNase H during the LAMP step to degrade DNA : RNA hybrids, significantly improving quantification accuracy[57] (Fig. 8B). Furthermore, this digital RT-LAMP method can be integrated with smartphone imaging for droplet counting, enabling convenient and robust detection[58] (Fig. 8C). To further enhance the speed and sensitivity of digital LAMP assays, a customized real-time digital nucleic acid amplification instrument was integrated with a SlipChip,[59] enabling the rapid measurement of

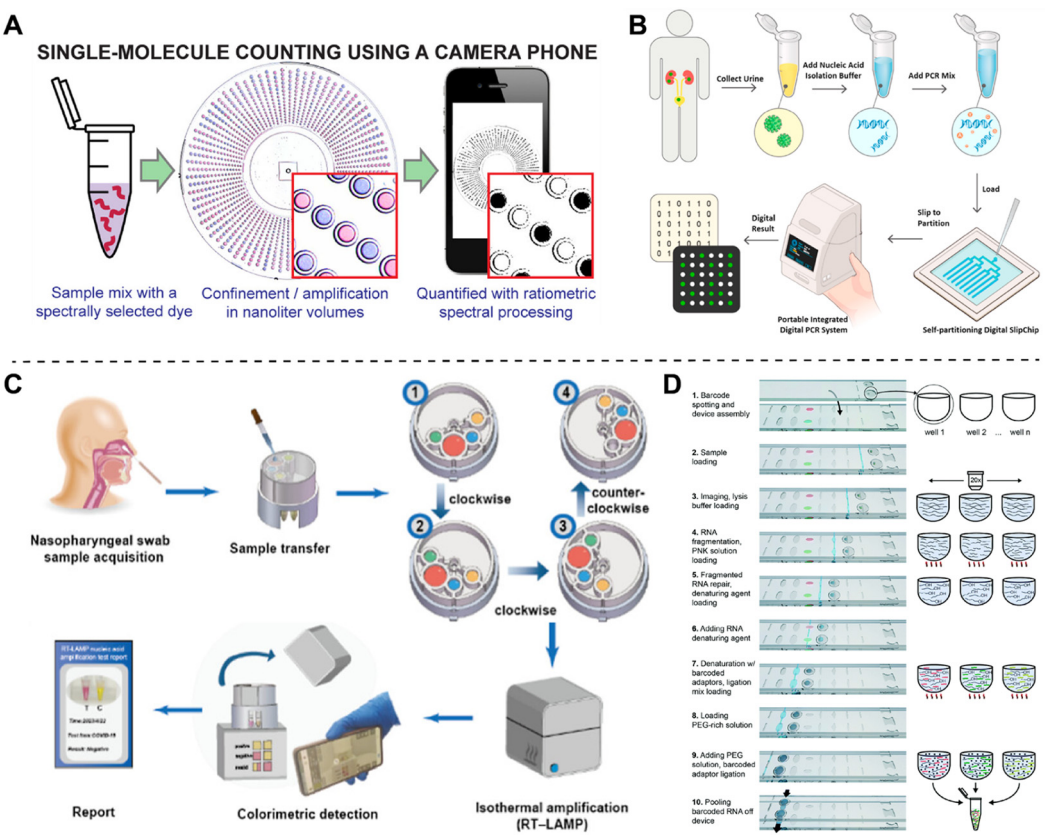

Fig. 9 Portable SlipChip systems for point-of-care testing (POCT). (A) SlipChip for single-molecule digital isothermal amplification with readout performed using a smartphone. Reproduced with permission from ref. 61. Copyright 2016, American Chemical Society. (B) Portable integrated digital PCR (PI-dPCR) system combining sp-SlipChip for absolute quantification of BK virus. Reproduced with permission from ref. 62. Copyright 2021, Elsevier. (C) Injection-moldable combination-lock SlipChip (cl-SlipChip) for integrated SARS-CoV-2 testing. Reproduced with permission from ref. 63. Copyright 2024, American Chemical Society. (D) Multistep device for multiplexed RNA sequencing. Reproduced with permission from ref. 22. Copyright 2019, Royal Society of Chemistry.

nucleic acid markers associated with antibiotic susceptibility in *E. coli* directly from clinical urine samples within 30 minutes[60] (Fig. 8D). Additional SlipChip designs have also been advanced for digital isothermal applications. The sp-SlipChip generated 2240 nanoliter droplets for digital LAMP quantification of HPV-16 and HPV-18 viral DNA[18] (Fig. 8E). More recently, the da-SlipChip was used to create tens of thousands of picoliter droplets for digital LAMP quantification of SARS-CoV-2 nucleic acids using a random-access system[19] (Fig. 8F).

Isothermal amplification is generally challenging to multiplex due to nonspecific amplification. Owing to the DNA-guided nucleic acid cleavage activity of argonaute (Ago) proteins, which enables one enzyme to specifically target multiple probe sequences. Luo *et al.* developed a parallel droplet-fusion SlipChip that utilized multiplex digital LAMP-Ago assays to achieve parallel viral load quantification of respiratory viruses, including SARS-CoV-2, influenza A, and influenza B.[24]

POCT nucleic acid analysis. Conventional digital nucleic acid analysis systems typically require precise fluidic control pumps, bulky fluorescence imaging modules, and thermal cycling units, which limit their applicability in point-of-care testing (POCT). In contrast, SlipChip technology eliminates the need for external fluidic control systems, thereby enabling digital genetic analysis in portable and low-resource settings. By using an unmodified camera phone for imaging combined with ratiometric image processing, Rodriguez-Manzano *et al.* achieved accurate single-molecule counting of digital LAMP reactions in SlipChip droplets with volumes as low as 5 nL, eliminating the need for specialized microscopic imaging equipment[61] (Fig. 9A). Xu *et al.* developed a portable integrated digital PCR (PI-dPCR) system by combining the sp-SlipChip with a compact integrated instrument, allowing bedside digital PCR quantification of BK virus in urine samples[62] (Fig. 9B). Furthermore, leveraging the SlipChip's capability for multistep fluid manipulation, an injection-moldable combination-lock SlipChip (cl-SlipChip) (Fig. 9C) was designed to integrate nucleic acid extraction, amplification, and detection into a palm-sized base station. This system enabled rapid detection of SARS-CoV-2 and HPV-16/18 from self-collected samples,[63,64] making it highly suitable for disease testing in resource-limited settings and even potential home use. Notably, SlipChip designs even allow milliliter-scale sample input, making them suitable for a broader range of point-of-care testing scenarios.[65]

In addition, SlipChip has been applied to other nucleic acid-related processes. Utilizing multistep sliding for droplet merging, the SlipChip platform has enabled high-throughput library preparation for RNA sequencing (RNAtag-Seq)[22] (Fig. 9D) as well as on-chip DNA synthesis and sequencing.[66] These developments further expand the versatility of SlipChip technology in the field of nucleic acid analysis.

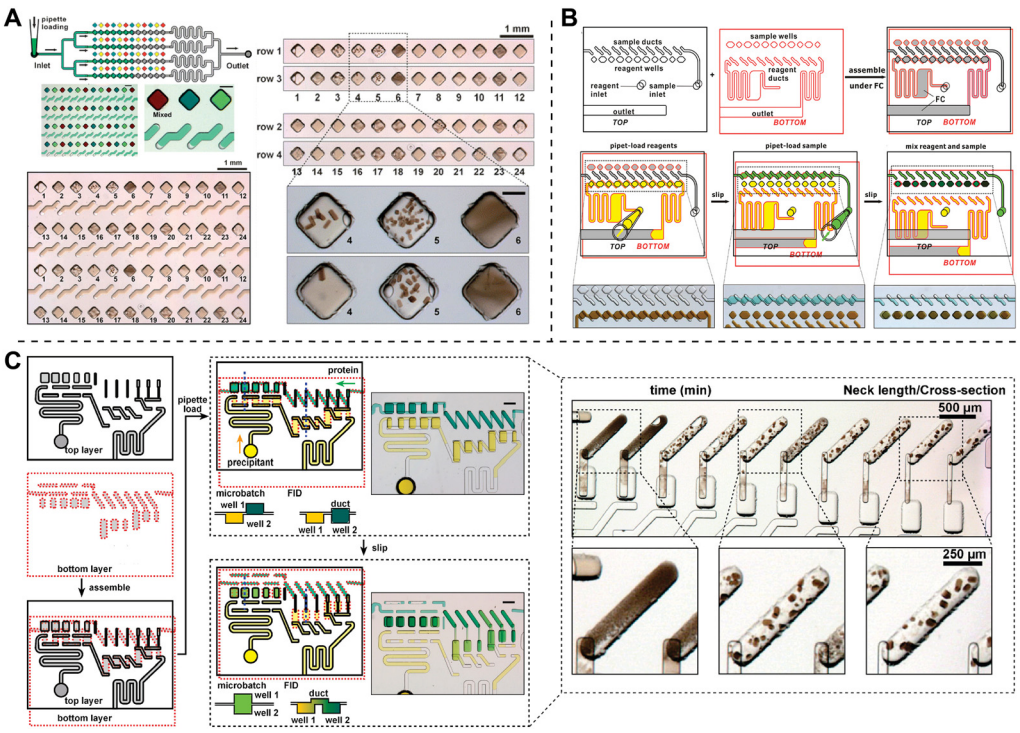

Fig. 10 SlipChip for study protein crystallization. (A) The original SlipChip for membrane protein crystallization screening with preloaded precipitants. Reproduced with permission from ref. 8. Copyright 2009, Royal Society of Chemistry. (B) A user-loaded SlipChip that permits manual introduction of precipitants and supports 16 parallel crystallization precipitants. Reproduced with permission from ref. 66. Copyright 2009, American Chemical Society. (C) A free-interface diffusion (FID) SlipChip that generates a concentration gradient for crystallization screening. Reproduced with permission from ref. 25. Copyright 2009, American Chemical Society.

4.2 Protein analysis

Protein crystallization. Protein crystallography typically requires screening hundreds of conditions while using only small amounts of protein. SlipChip technology provides a powerful high-throughput tool for exploring protein crystallization conditions. By pre-embedding different reagents in microchambers and subsequently introducing protein solutions that were mixed through sliding, the original SlipChip demonstrated screening of membrane protein crystallization[8] (Fig. 10A). Later, by using two independent channels for the separate introduction of protein and precipitant solutions and adjusting the dimensions of the upper and lower microchambers to control the mixing ratios, a user-loaded SlipChip (Fig. 10B) enabled the parallel screening of protein samples against 16 different precipitants, each with 11 distinct mixing ratios.[67] Furthermore, by integrating the free-interface diffusion method, the SlipChip could test 16 precipitants against a single protein sample under five different equilibration times to study protein nucleation kinetics (Fig. 10C). By changing the diffusion distance and the cross-sectional area of the diffusion channels, the device increased the likelihood of identifying optimal conditions for crystal formation.[25] The protein crystals obtained using SlipChip were verified to be reliable by X-ray diffraction analysis. The integration of SlipChip technology with protein production, characterization, and *in situ* diffraction could contribute to advancing protein structure determination.[68]

Functional immunoassay. Protein immunoassays have also been implemented on SlipChip platforms, enabling diverse functionalized protein testing. By performing bead-based heterogeneous immunoassays within the SlipChip at nanoliter scales, highly sensitive batch detection of an insulin immunoenzymatic assay was achieved, with a detection limit of approximately 13 pM (ref. 69) (Fig. 11A). In addition to fluorescence-based readouts, enzyme-linked immunosorbent assays (ELISA) have been adapted to SlipChip to enable visual and quantitative detection.

Song *et al.* developed a multiplex volumetric bar-chart chip (V-Chip), in which catalase was used as the ELISA probe. The oxygen generated during the reaction propelled

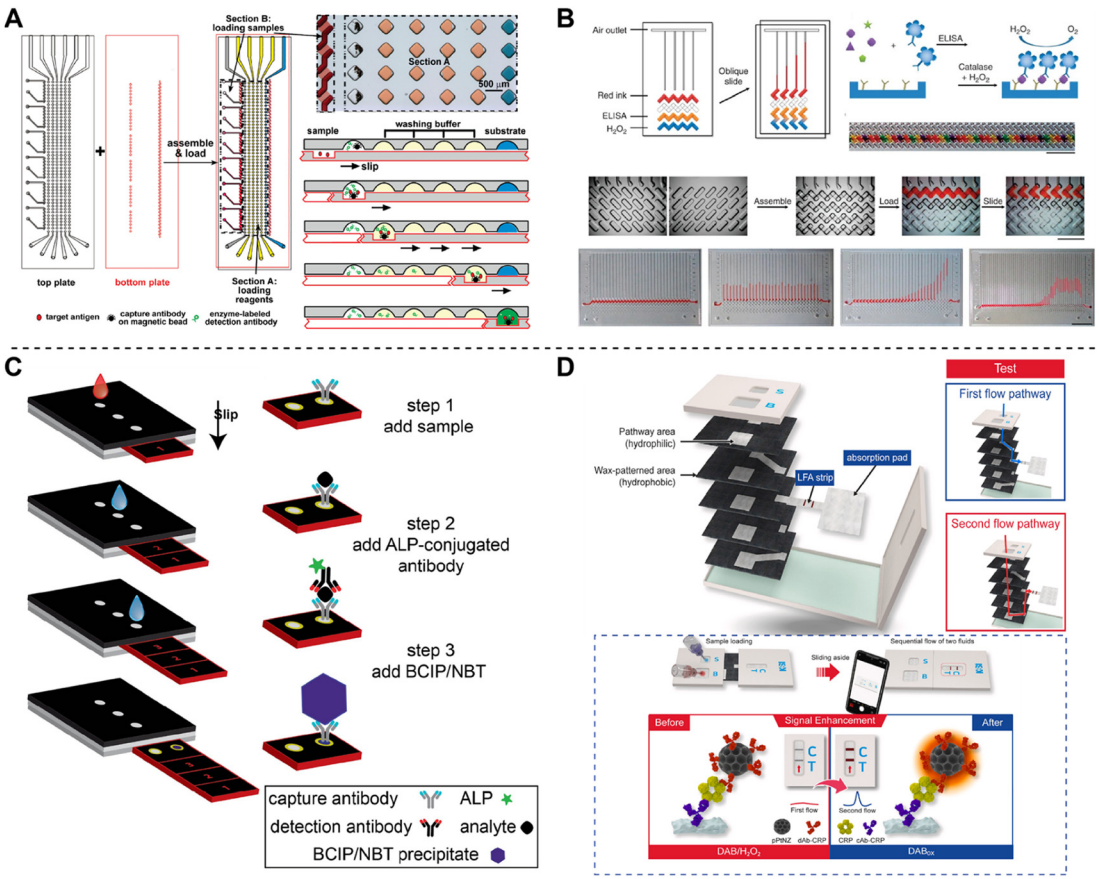

Fig. 11 SlipChip applications for functional immunoassay. (A) Performing heterogeneous immunoassays with multiple nanoliter samples in SlipChip. Reproduced with permission from ref. 69. Copyright 2010, American Chemical Society. (B) A multiplex volumetric bar-chart chip (V-Chip) for visualized ELISA reaction. Reproduced with permission from ref. 70. Copyright 2012, Springer Nature. (C) Schematic of a paper-based SlipChip device performing ELISA for rapid C-reactive protein detection. Reproduced with permission from ref. 71. Copyright 2018, Elsevier. (D) Working principle of the platinum nanozyme-enhanced SlipChip (pPtNZ-SlipChip) for CRP immunoassay. Reproduced with permission from ref. 72. Copyright 2023, Elsevier.

preloaded ink bars, providing visualized bar-chart quantification of multiple protein biomarkers[70] (Fig. 11B). Paper-based immunoassays on SlipChip have also been utilized for protein detection in point-of-care testing, owing to their portability and low cost. By storing reagents (capture antibodies, detection antibodies, substrates, and buffers) in isolated regions and manually sliding the strip to sequentially bring reagents into contact after adding the sample and water, Verma *et al.* developed a sliding-strip microfluidic device that performs ELISA on paper for rapid C-reactive protein (CRP) detection[71] (Fig. 11C). Paper-based SlipChip can also function in conventional lateral flow assay (LFA). By immobilizing CRP capture antibodies onto the test line and utilizing porous platinum nanozymes (pPtNZs) to catalyze diaminobenzidine (DAB) for signal amplification, Son *et al.* reported a nanozyme-amplified SlipChip capable of detecting CRP concentrations as low as 0.03 ng mL^{-1} within 20 minutes[72] (Fig. 11D). These developments further demonstrate the potential of SlipChip platforms for on-site and point-of-care protein testing.

Digital immunoassay. To further realize absolute quantification of proteins, digital immunoassays based on SlipChip platforms have been developed. Compared with conventional chemiluminescence methods, digital immunoassays improve detection sensitivity by 3–4 orders of magnitude. The concept of digital immunoassay was first proposed by Rissin *et al.* as the single-molecule array (Simoa).[73] In this approach, target proteins are captured by antibody-coated beads, then labeled with enzyme reporters that catalyze fluorescent reactions. Each bead carries either zero or one target molecule, and is subsequently compartmentalized into femtoliter wells containing fluorogenic substrates, generating digital readouts that enable absolute quantification of low-abundance proteins. Building upon this principle, Ge *et al.* developed a SlipChip-based digital immunoassay using Brownian trapping with drift[74] (Fig. 12A), which significantly extended the dynamic range up to 4×10^7 and achieved a sensitivity of 20 molecules per 3 μL sample. However, in traditional digital immunoassays, pre-mixing of immune-complex-carrying beads with fluorescent substrates can prematurely trigger enzymatic reactions, resulting in high background signals. To address this issue, Lyu *et al.* developed a bead-based SlipChip (bb-SlipChip) (Fig. 12B) that separates the loading of beads and substrates and initiates reactions through controlled sliding, effectively suppressing background

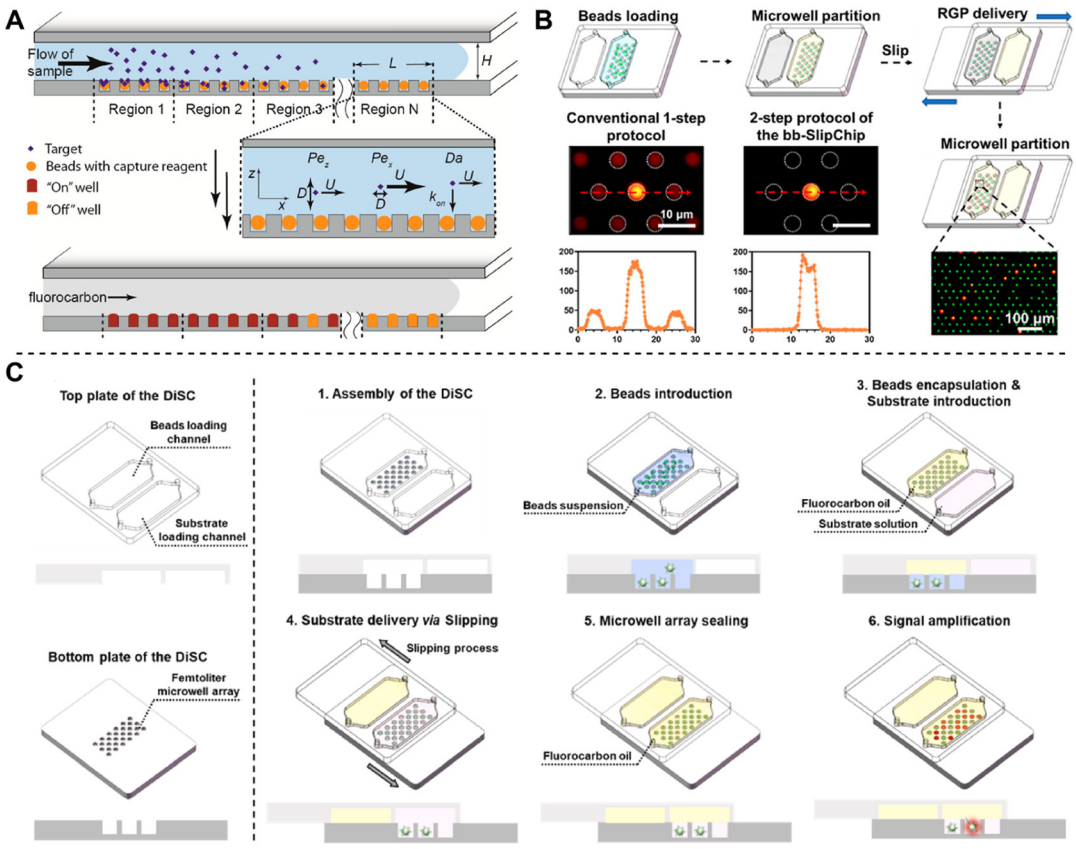

Fig. 12 SlipChip applications for digital immunoassays. (A) Working principle of the high-dynamic-range digital immunoassay based on Brownian trapping with drift. Reproduced with permission from ref. 74. Copyright 2014, American Chemical Society. (B) Working principle of the digital immunoassay using the bb-SlipChip. Reproduced with permission from ref. 20. Copyright 2023, American Chemical Society. (C) Digital immunoassay on a SlipChip (DiSC) for quantitative analysis of a potential serum protein biomarker, spondin-1 (SPON1). Reproduced with permission from ref. 76. Copyright 2024, Elsevier.

fluorescence and markedly improving the signal-to-noise ratio. By integrating fluorescence-encoded microspheres,[75] the bb-SlipChip enabled duplex digital detection of IL-6 and IL-10 with detection limits as low as 5.2 and 15.3 fg mL^{-1}, respectively. Furthermore, the bb-SlipChip has been applied to evaluate spondin-1 (SPON1) as a potential serum biomarker for ovarian cancer liquid biopsy[20,76] (Fig. 12C).

Protein separation and identification. High-throughput and rapid protein separation has long been a central goal in proteomics. Integrating protein separation and identification approaches into SlipChip platforms enables fast and efficient on-chip proteomic analysis. Hassan *et al.* developed a droplet-interface microchip electrophoresis (MCE) SlipChip platform composed of two plastic plates: one containing droplet reservoirs and the other integrating precast agarose or polyacrylamide gel separation channels. Parallel electrophoresis performed on the SlipChip permitted high-throughput separation of nucleic acids and protein biomolecules encapsulated within droplets[40] (Fig. 13A). Isoelectric focusing (IEF) is a powerful and widely used technique for protein separation and purification. Zhao *et al.* designed a microfluidic SlipChip that focuses protein analytes in a microchannel and then partitions the focused bands into discrete droplets by sliding the plates[77] (Fig. 13B). The separated droplets can be directly recovered or processed on-chip for further analysis. Building upon this concept, Wang *et al.* further integrated matrix-assisted laser desorption/ionization time-of-flight mass spectrometry (MALDI-TOF MS) by employing soda-lime glass as the SlipChip substrate. After IEF and droplet partitioning, the device could be opened for *in situ* MALDI-TOF MS, enabling direct on-chip protein identification without sample transfer[78] (Fig. 13C).

4.3 Microbial analysis

Antimicrobial susceptibility testing. Conventional clinical antimicrobial susceptibility testing (AST) methods are often limited by low throughput and long turnaround times. SlipChip is well-suited for bacterial culture, as confinement within microdroplets accelerates bacterial growth to threshold concentrations. To simplify and accelerate the AST process, Yi *et al.* developed a DEP-AST SlipChip that integrates dielectrophoresis (DEP), SlipChip technology, droplet arrays, and microscopic image analysis into a compact and portable system (Fig. 14A). This device enables direct bacterial isolation from positive blood cultures using DEP, followed by parallel inoculation of bacteria into nanoliter broth droplets containing different antibiotics *via* a sliding step. By monitoring bacterial growth kinetics under a microscope, reliable AST results consistent with standard broth microdilution tests can be obtained within 3–8 hours.[79]

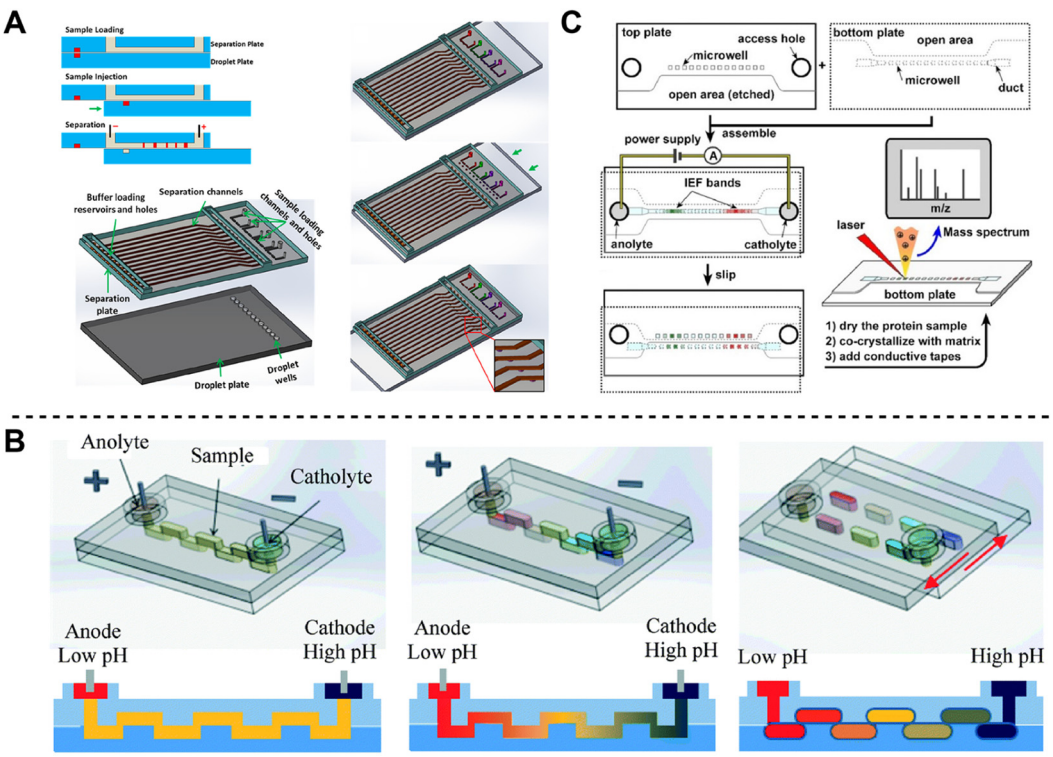

Fig. 13 SlipChip applications for protein separation and identification. (A) 3D schematic showing the working principle of electrophoresis on the SlipChip. Reproduced with permission from ref. 40. Copyright 2015, American Chemical Society. Reproduced with permission from ref. 77. Copyright 2013, Royal Society of Chemistry. (B) Schematic drawing of IEF separation and *in situ* compartmentalization in a SlipChip. (C) Schematic operation of the sIEF-MALDI SlipChip device for *in situ* protein analysis. Reproduced with permission from ref. 78. Copyright 2014, Wiley-VCH GmbH.

Moreover, by preloading antibiotics on the SlipChip, the testing throughput was significantly improved, enabling up to 192 AST assays to be completed within 3 hours (ref. 30) (Fig. 14B). Other SlipChip variants such as the nano-dilution SlipChip,[32] capable of generating multiple dilution gradients, have been successfully applied to rapid AST (Fig. 14C). To further achieve stable antibiotic concentration gradients for determining the minimum inhibitory concentration (MIC), Wan *et al.* designed a rotating SlipChip (RSC) incorporating a three-dimensional circular "Christmas tree" microfluidic

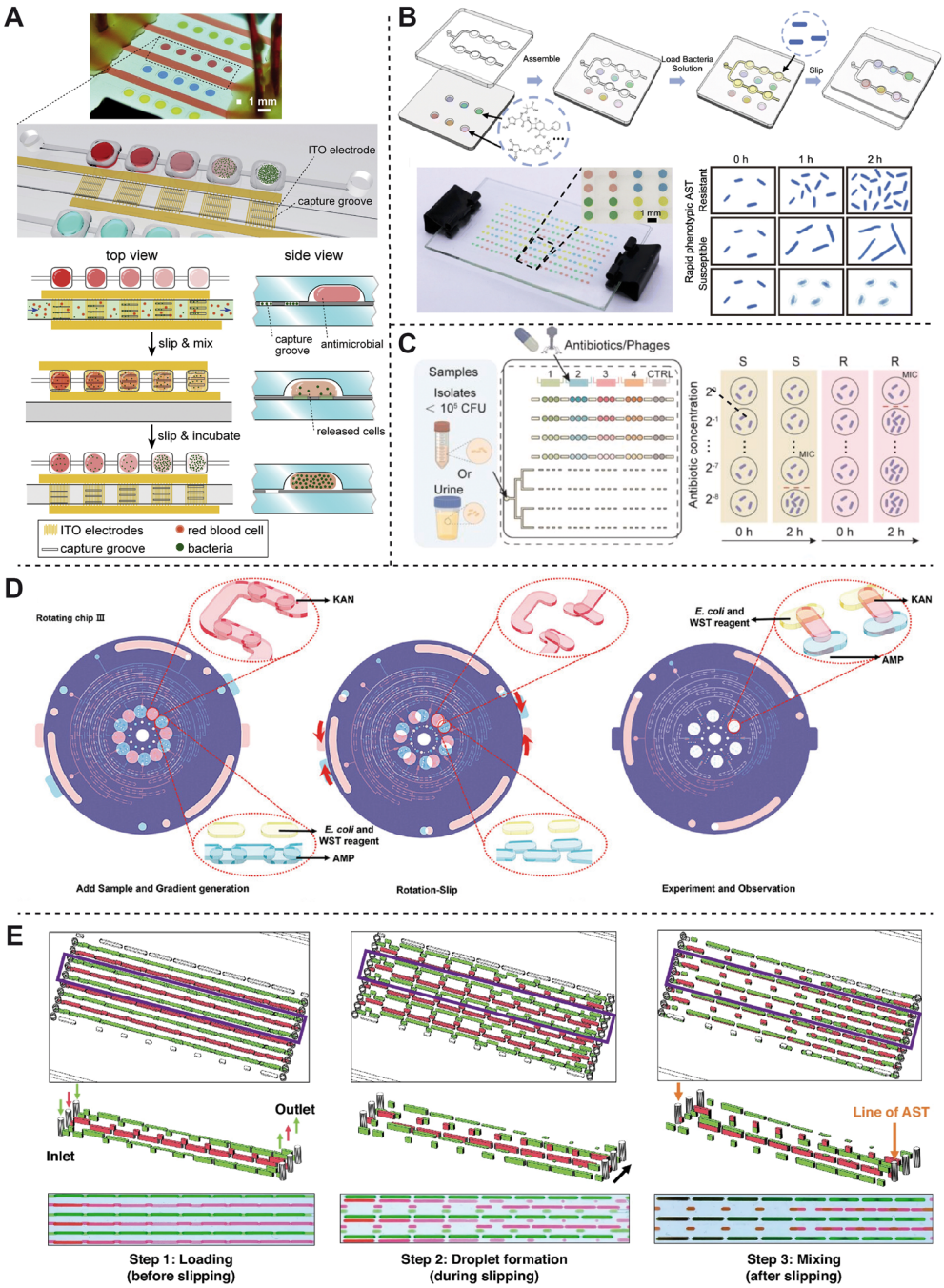

Fig. 14 SlipChip applications in antimicrobial susceptibility testing (AST). (A) SlipChip integrated with dielectrophoresis (DEP) for direct bacterial separation from blood cultures and subsequent AST. Reproduced with permission from ref. 79. Copyright 2019, Elsevier. (B) Antibiotic-preloaded SlipChip for high-throughput AST. Reproduced with permission from ref. 30. Copyright 2022, Royal Society of Chemistry. (C) Nano-dilution SlipChip enabling stepwise dilution to generate antibiotic concentration gradients for AST. Reproduced with permission from ref. 32. Copyright 2025, Elsevier. (D) Rotating SlipChip (RSC) with a three-dimensional circular "Christmas tree" structure for bacterial minimum inhibitory concentration (MIC) determination. Reproduced with permission from ref. 80. Copyright 2024, Wiley-VCH GmbH. (E) A schematic diagram demonstrating the working principle of the self-dilution for faster antimicrobial susceptibility testing (SDFAST) device for AST. Reproduced with permission from ref. 81. Copyright 2025, Springer Nature.

gradient generator (Fig. 14D). The device can be self-sealed under ambient pressure and allows rapid MIC determination within 4 hours.[80] Wat *et al.* developed a microfluidic device named self-dilution for faster antimicrobial susceptibility testing (SDFAST), which utilizes an array of discrete chambers with varying volumes to automatically generate a dilution series for antimicrobial susceptibility testing (AST). By integrating the chip with a colorimetric water-soluble tetrazolium-8 (WST-8) assay, the system produces clear readouts based on color intensity after only 4–6 hours of incubation[81] (Fig. 14E). These developments demonstrate that SlipChip technology offers a versatile and effective

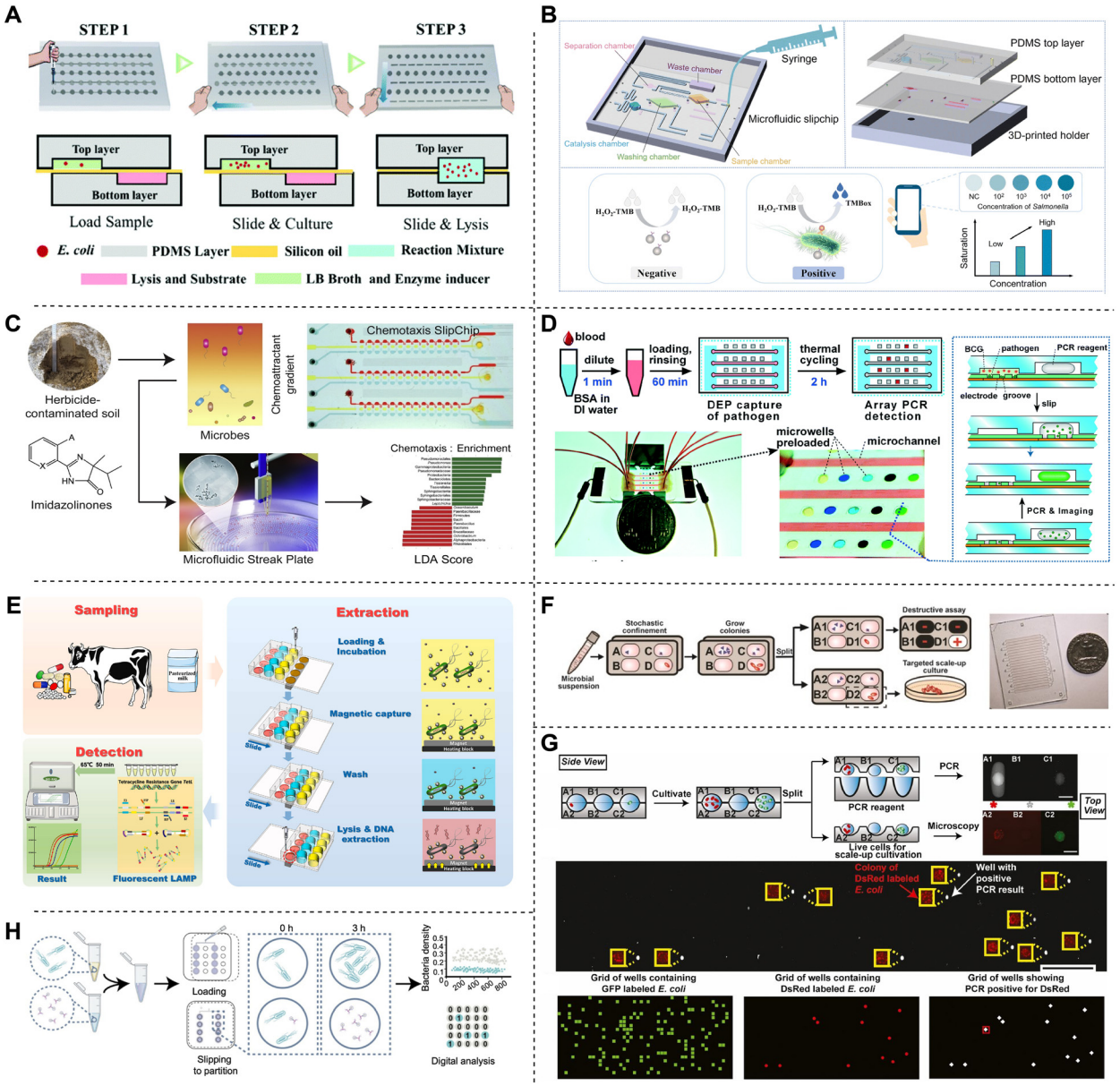

Fig. 15 Application of SlipChip in microbial isolation and identification. (A) SlipChip for rapid bacterial detection based on bacterial growth and β-glucuronidase (GUS) enzymatic activity. Reproduced with permission from ref. 82. Copyright 2021, Royal Society of Chemistry. (B) Schematic of the all-in-one microfluidic SlipChip for biosensing of *Salmonella*. Reproduced with permission from ref. 83. Copyright 2024, Royal Society of Chemistry. (C) SlipChip platform for studying bacterial chemotaxis and isolating pollutant-degrading microbial genera. Reproduced with permission from ref. 84. Copyright 2018, Elsevier. (D) SlipChip integrated with dielectrophoresis (DEP) for bacterial separation f and multiplex array PCR for species identification. Reproduced with permission from ref. 85. Copyright 2014, Royal Society of Chemistry. (E) Schematic illustration of SlipChip-based IMS-LAMP assay for isolation and detection of *B. cereus* with tetracycline resistance gene tetL in pasteurized milk. Reproduced with permission from ref. 86. Copyright 2025, Elsevier. (F) A splitting SlipChip for single-bacterial culture and generation of two identical replicates through droplet splitting. Reproduced with permission from ref. 88. Copyright 2014, Royal Society of Chemistry. (G) Isolation and cultivation of pure microcolonies from mixed populations followed by PCR-based identification of specific strains. Reproduced with permission from ref. 89. Copyright 2025, *PNAS*. (H) A digital phage SlipChip (dp-SlipChip) for the quantification of infectious bacteriophages. Reproduced with permission from ref. 90. Copyright 2023, American Chemical Society.

platform for developing rapid, high-throughput, and reliable phenotypic AST methods.

Microbial isolation and identification. The SlipChip platform provides an integrated strategy for microbial isolation and identification, enabling rapid and multiplexed analysis through multiple technical routes. The enzymatic activity of metabolic enzymes, such as β-D-glucuronidase (GUS), during bacterial growth can be exploited for rapid bacterial identification and detection[82] (Fig. 15A). Furthermore, Xue *et al.* developed an all-in-one microfluidic SlipChip, which integrates immunomagnetic nanobeads (IMBs) for bacterial capture with immuno-Au@PtPd nanocatalysts (INC) for signal generation. This integrated system enables the rapid detection of *Salmonella* with a detection limit as low as 101.2 CFU mL^{-1} within 30 min (ref. 83) (Fig. 15B). By preloading microchambers with varying concentrations of imazapyr-based compounds and culturing bacteria on the device, the SlipChip platform can been applied to study bacterial chemotaxis and isolate microbial genera capable of degrading environmental pollutants[84] (Fig. 15C). By integrating dielectrophoresis (DEP) for bacterial capture with nanoliter-scale multiplex array PCR for species identification, Cai *et al.* successfully achieved simultaneous isolation and identification of *Pseudomonas aeruginosa*, *Staphylococcus aureus*, and *Escherichia coli O157:H7* directly from human whole blood and contaminated water within 3 hours (ref. 85) (Fig. 15D). In addition, by combining immunomagnetic separation (IMS) with LAMP, Li *et al.* isolated and identified *Bacillus cereus* carrying the tetracycline resistance gene *tetL* from pasteurized milk, reaching a detection limit of 21.5 CFU mL^{-1} within 2 h (ref. 86) (Fig. 15E).

SlipChip devices have also been demonstrated to enable random single-cell or single-bacterium isolation for culture and downstream analysis.[87] Ma *et al.* developed a splitting SlipChip that encapsulates and cultures bacteria at the single-cell level, then divides droplets through sliding to generate two identical replicas of each microcolony array for subsequent analysis or scaled-up culture[88] (Fig. 15F). Furthermore, because each microwell position on a SlipChip can be spatially indexed, when coupled with genomic assays such as PCR, this approach enables gene-targeted microfluidic cultivation from complex mixtures, as validated by the isolation of a gut bacterium listed among the Human Microbiome Project's "Most Wanted" taxa[89] (Fig. 15G). This method has also been applied to isolate previously

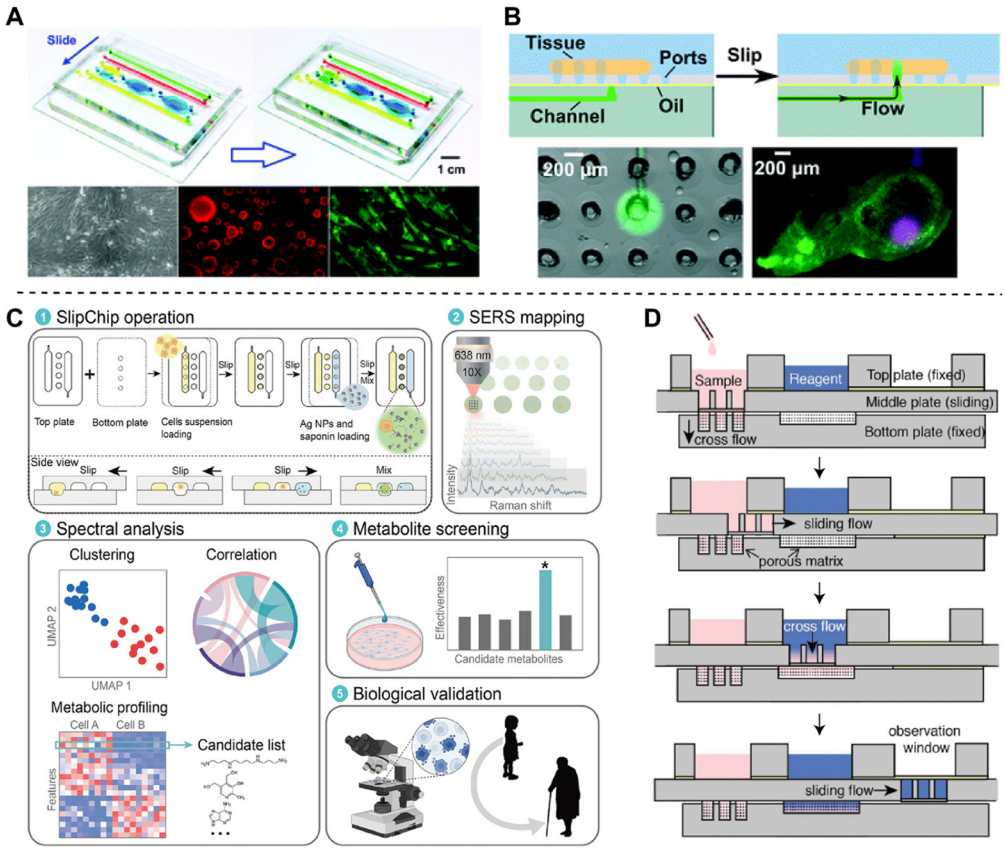

Fig. 16 SlipChip for cell assays. (A) PDMS-based SlipChip for mammalian cell culture. Reproduced with permission from ref. 37. Copyright 2015, Royal Society of Chemistry. (B) A movable-port SlipChip device for localized stimulation of live tissues. Reproduced with permission from ref. 91. Copyright 2018, Royal Society of Chemistry. (C) Single-cell metabolic analysis using an integrated SlipChip-SERS (surface-enhanced Raman spectroscopy) microfluidic platform. Reproduced with permission from ref. 92. Copyright 2024, Wiley-VCH GmbH. (D) Cross-sectional schematic of Slip-X-Chip and its operation. Reproduced with permission from ref. 93. Copyright 2022, IEEE.

"unculturable" microorganisms from human clinical samples. Finally, SlipChip technology has been further extended to single biological assays. Li *et al.* developed a digital phage SlipChip (dp-SlipChip) that partitions bacteriophages and host bacteria into 2304 droplets of 3 nL each. By monitoring bacterial growth dynamics over three hours, the system accurately quantified infectious phage particles[90] (Fig. 15H).

4.4 Cell assays

Furthermore, SlipChip technology has been extended to cell culture and single-cell analysis. For cell culture applications, SlipChip fabricated from PDMS is highly compatible with mammalian cell growth and enable cytokine detection[37] (Fig. 16A). In addition to isolated cells, Megan A. Catterton *et al.* developed a SlipChip featuring a movable microfluidic port that allows localized stimulation of live tissue or organ cultures (Fig. 16B). By creating a movable port beneath the chip and integrating a tissue chamber supported by a permeable scaffold, this design enables precise, user-defined stimulation of specific tissue regions.[91] Leveraging the capability of multistep droplet manipulation, Liu *et al.* integrated surface-enhanced Raman spectroscopy (SERS) with SlipChip to achieve single-cell metabolic profiling. Using this SlipChip–SERS platform (Fig. 16C), twelve distinct metabolites were identified from primary human fibroblasts, among which spermine was verified as an effective inducer of cellular senescence.[92] Beyond the conventional two-plate SlipChip architecture, Iseri *et al.* recently introduced the Slip-X-Chip,[93] a sliding microfluidic platform composed of three plates. In addition to lateral plate-to-plate sliding for fluid routing, vertically aligned through-holes across the three plates enable capillary-driven transport from the upper to the lower wells (Fig. 16D). Using this design, the authors demonstrated on-chip enrichment and compartmentalization of human glioblastoma cells, followed by single-well viability analysis directly from unprocessed samples.

4.5 Materials and particle synthesis

Beyond the scope of biological analysis, SlipChip also holds great potential as parallelized arrays of microreactors for material synthesis. By isolating reagents within nanoliter-scale droplets, SlipChip can simultaneously initiate polymerization reactions or nanoparticle synthesis across multiple independent compartments. Through precise design of the microcavity geometry on the top and bottom plates, Qu *et al.* utilized the SlipChip platform to fabricate on-demand micro-parts (mPods) with finely controlled sizes and shapes, as well as bilayer Janus microparts[94] (Fig. 17A). Furthermore, the ability of SlipChip to generate microstructures with customizable geometries has also been explored for fabricating personalized nanoscale anti-counterfeiting label. By mixing gap-enhanced Raman tags (GERTs) with liquid resin, SlipChip has been employed to produce physically unclonable, anti-counterfeiting orthogonal Raman labels in various shapes such as, circular, triangular, and square labels[95] (Fig. 17B), as well as hollow rectangular "SJTU" micro-patterns[96] (Fig. 17C), demonstrating their unique capability in advanced materials manufacturing.

5 Discussion and future directions

The SlipChip has emerged as a distinct and influential branch of microfluidic technology, offering a versatile strategy for performing complex fluidic operations without external pumps or valves. Its core principle, controlled slipping between two microstructured plates, enables precise and reconfigurable liquid manipulation by toggling between connected and disconnected fluidic states. This straightforward mechanical operation not only simplifies system architecture but also improves device robustness and portability, making the platform especially valuable for applications in resource-limited environments. Over the past decade, innovations in SlipChip design, materials, and fabrication have expanded its utility across chemical analysis, molecular diagnostics, single-cell biology, and materials synthesis. As a result, the SlipChip has established itself as a scalable and practical microfluidic system that bridges the gap between high-precision laboratory workflows and point-of-care simplicity.

Despite its versatility, several technical challenges must be addressed to fully realize the potential of SlipChip technology. One key limitation lies in the manual operation commonly used for plate slipping, which restricts reproducibility and throughput. Transitioning to automated or semi-automated actuation, such as through motorized stages,[97] programmable linear drives, or integrated frames[43] would enable more controlled and consistent sliding, improving both precision and usability in complex multi-step workflows. In parallel, further investigation into fundamental design principles, including microfeature geometry, surface chemistry, and inter-plate gap dynamics, is needed to enhance device performance and reliability. The gap between plates, in particular, remains a critical and often variable parameter influencing fluid behavior, evaporation, and cross-contamination.

From a fabrication standpoint, while etching-based methods in glass or silicon are well-suited for prototyping, they are less amenable to mass production. Future efforts should prioritize scalable manufacturing routes such as injection molding and advanced 3D printing, which promise higher throughput and lower per-device costs, albeit with trade-offs in microstructural resolution and surface finish. Additionally, improvements in device assembly and microalignment, such as through self-aligning structures or integrated guiding features, would facilitate more reproducible and user-friendly operation.

Looking forward, several promising directions could further extend the functionality and application scope of SlipChip systems. The platform's ability to switch between continuous and discrete fluidic environments makes it

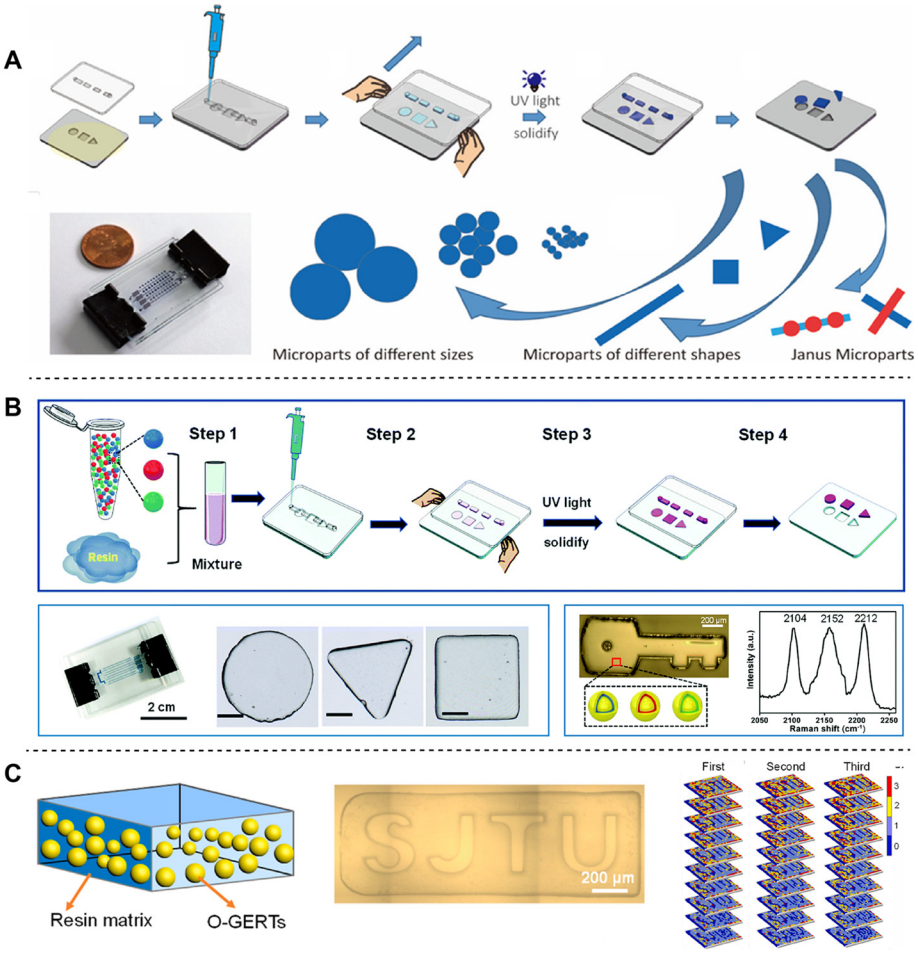

Fig. 17 Application of SlipChip in materials and particle synthesis. (A) Schematic of the microfluidic SlipChip molding method for generating microparticles on demand (mPods). Reproduced with permission from ref. 94. Copyright 2019, American Chemical Society. (B) Schematic of the fabrication process for anti-counterfeiting Raman labels using the SlipChip technique. Reproduced with permission from ref. 95. Copyright 2022, Royal Society of Chemistry. (C) Representative Raman labels featuring the "SJTU" pattern. Reproduced with permission from ref. 96. Copyright 2022, De Gruyter.

inherently compatible with other separation and analysis techniques, such as electrophoresis, Western blotting, and isoelectric focusing. Moreover, the spatially fixed, two-dimensional array architecture of SlipChip is ideally suited for spatial analysis and multiplexed screening.[98] Functions such as droplet splitting and merging open doors to multi-omics studies,[99] single-cell interaction analysis, and high-throughput synthetic biology screening.[100]

The SlipChip platforms show strong potential for system-level integration with upstream sample preparation steps, such as cell lysis, nucleic acid extraction, and purification, enabling more complete sample-to-answer workflows. In addition, integration with portable readers and standardized interfaces could enable a universal "reader-holster" system, where a single instrument supports multiple SlipChip assay cartridges, an important step toward standardized point-of-care deployment. Incorporating artificial intelligence for image analysis and data integration could further enhance analytical capabilities,[101] especially when combined with other detection modalities such as sequencing, Raman spectroscopy[102] or mass spectrometry.[103] Finally, surface functionalization within individual wells, for selective molecule or cell capture, coupled with improved methods for targeted recovery of specific compartments, would enable more sophisticated on-chip assays and facilitate off-chip validation.

In summary, while the SlipChip platform has already demonstrated broad utility, ongoing advances in automation, fabrication, functional integration, and standardization will be essential to unlock its full potential in both research and clinical settings. By addressing these challenges and pursuing these future directions, SlipChip technology is poised to become an even more powerful and accessible tool for the next generation of microfluidic applications.

Conclusions

In conclusion, the SlipChip exemplifies a unique microfluidic platform in which simple sliding motion enables complex fluid operations without pumps or valves. Since 2009, it has

evolved into diverse architectures, supporting applications such as protein crystallization, digital PCR, immunoassays, and single-cell analysis. With improvements in fabrication, automation, and fluidic precision, SlipChip is poised to play an increasingly important role in precision medicine, high-throughput screening, and biological research. Its continued development promises accurate, efficient, and cost-effective solutions, bridging the gap between laboratory experiments and practical applications.

Author contributions

The manuscript was written through contributions of all authors. Yang Luo wrote original draft, visualization, reviewed, and edited. Weijie Yuan wrote original draft, visualization. Sujin Jung reviewed and edited. Feng Shen performed conceptualization, writing, visualization, supervision, project administration, funding acquisition.

Conflicts of interest

There are no conflicts to declare.

Data availability

No primary research results, software or code have been included and no new data were generated or analysed as part of this review.

Acknowledgements

This work was supported by the Natural Science Foundation of Shanghai (No. 23ZR1432900), the Interdisciplinary Program of Shanghai Jiao Tong University (No. YG2024QNA45, No. YG2025ZD16), the National Natural Science Foundation of China (No. 32470086), the National Natural Science Foundation of China (No. 32171463).

Notes and references

1 B. Sharma and A. Sharma, *Adv. Eng. Mater.*, 2022, **24**, 2100738.
2 Y. Ding, P. D. Howes and A. J. deMello, *Anal. Chem.*, 2020, **92**, 132–149.
3 Y. Zheng, H. Shi, Z. Tan, W. Xu, R. Zhao, Z. Dan, Z. Dai, J. Liao and H. Wu, *TrAC, Trends Anal. Chem.*, 2025, **188**, 118236.
4 X. Liu, D. Ma, H. Ye, Y. Hou, X. Bai, Y. Xing, X. Cheng, B. Lin and Y. Lu, *TrAC, Trends Anal. Chem.*, 2023, **166**, 117153.
5 H. Yuan, Z. Miao, C. Wan, J. Wang, J. Liu, Y. Li, Y. Xiao, P. Chen and B.-F. Liu, *Lab Chip*, 2025, **25**, 1015–1046.
6 E. Noviana, T. Ozer, C. S. Carrell, J. S. Link, C. McMahon, I. Jang and C. S. Henry, *Chem. Rev.*, 2021, **121**, 11835–11885.
7 Y. Song, Y. Zhou, K. Zhang, Z. Fan, F. Zhang and M. Wei, *Lab Chip*, 2024, **24**, 4483–4513.
8 W. Du, L. Li, K. P. Nichols and R. F. Ismagilov, *Lab Chip*, 2009, **9**, 2286–2292.
9 W. Lyu, M. Yu, H. Qu, Z. Yu, W. Du and F. Shen, *Biomicrofluidics*, 2019, **13**, 041502.
10 Q. Luo, Z. Yu, W. Lyu, Y. Luo, L. Xu and F. Shen, *Adv. Sens. Res.*, 2025, **4**, e00030.
11 M. Shen, Q. Wang, Q. Luo, J. Zhao and F. Shen, *Sens. Diagn.*, 2026, **5**, 26–41.
12 D. García Alonso, M. Yu, H. Qu, L. Ma and F. Shen, *Adv. Biosyst.*, 2019, **3**, 1900003.
13 J. Tong, F. Yin, M. Liang, W. Zong, Y. Wang, D. Xiao, J. Yin and Y. Mu, *TrAC, Trends Anal. Chem.*, 2025, **191**, 118299.
14 L. Li, M. A. Karymov, K. P. Nichols and R. F. Ismagilov, *Langmuir*, 2010, **26**, 12465–12471.
15 R. R. Pompano, C. E. Platt, M. A. Karymov and R. F. Ismagilov, *Langmuir*, 2012, **28**, 1931–1941.
16 R. R. Pompano, C. E. Platt, M. A. Karymov and R. F. Ismagilov, *Biophys. J.*, 2012, **102**, 187a.
17 F. Shen, W. Du, J. E. Kreutz, A. Fok and R. F. Ismagilov, *Lab Chip*, 2010, **10**, 2666–2672.
18 Z. Yu, W. Lyu, M. Yu, Q. Wang, H. Qu, R. F. Ismagilov, X. Han, D. Lai and F. Shen, *Biosens. Bioelectron.*, 2020, **155**, 112107.
19 W. Lyu, J. Zhang, Y. Yu, L. Xu and F. Shen, *Lab Chip*, 2021, **21**, 3086–3093.
20 W. Lyu, J. Yi, Q. Guo, Y. Wang, J. Zhang, T. Sun, H. Ma, T. Tang, X. Quan, H. Xu, F. Shen and H. Gu, *ACS Nano*, 2023, **17**, 12641–12651.
21 F. Shen, E. K. Davydova, W. Du, J. E. Kreutz, O. Piepenburg and R. F. Ismagilov, *Anal. Chem.*, 2011, **83**, 3533–3540.
22 D. V. Zhukov, E. M. Khorosheva, T. Khazaei, W. Du, D. A. Selck, A. A. Shishkin and R. F. Ismagilov, *Lab Chip*, 2019, **19**, 3200–3211.
23 Z. Yu, L. Xu, W. Lyu and F. Shen, *Lab Chip*, 2022, **22**, 2954–2961.
24 Y. Luo, X. Ye, N. Shen, L. Xu, J. Zhang, Z. Sheng, Q. Liu, Y. Feng and F. Shen, *Anal. Chem.*, 2025, **97**, 731–740.
25 L. Li, W. Du and R. F. Ismagilov, *J. Am. Chem. Soc.*, 2010, **132**, 112–119.
26 C. Shen, P. Xu, Z. Huang, D. Cai, S.-J. Liu and W. Du, *Lab Chip*, 2014, **14**, 3074–3080.
27 X. Liu, X. Li, N. Wu, Y. Luo, J. Zhang, Z. Yu and F. Shen, *ACS Sens.*, 2022, **7**, 1977–1984.
28 S. Begolo, F. Shen and R. F. Ismagilov, *Lab Chip*, 2013, **13**, 4331–4342.
29 F. Shen, W. Du, E. K. Davydova, M. A. Karymov, J. Pandey and R. F. Ismagilov, *Anal. Chem.*, 2010, **82**, 4606–4612.
30 X. Li, X. Liu, Z. Yu, Y. Luo, Q. Hu, Z. Xu, J. Dai, N. Wu and F. Shen, *Lab Chip*, 2022, **22**, 3952–3960.
31 M. Yu, X. Chen, H. Qu, L. Ma, L. Xu, W. Lv, H. Wang, R. F. Ismagilov, M. Li and F. Shen, *Anal. Chem.*, 2019, **91**, 8751–8755.
32 Q. Wang, X. Li, Y. a. Ren, Q. Hu, L. Xu, W. Chen, J. Liu, N. Wu, M. Tao, J. Sun, Y. Xu and F. Shen, *Biosens. Bioelectron.*, 2025, **271**, 117084.
33 J. Yang, Y. Deng, M. Zhang, S. Feng, S. Peng, S. Yang, P. Liu, G. Cai and G. Ge, *Biosensors*, 2023, **13**, 274.

34 Q. Wang, M. Wang, W. Lyu, X. Li, L. Xu, Y. Qin, Y. a. Ren, Z. Deng, M. Tao, W. Xiao and F. Shen, *Small Methods*, 2025, **9**, 2402045.
35 X.-H. Yan, L. Hu, Y. Li, X.-J. Feng and B.-F. Liu, *Chin. J. Anal. Chem.*, 2015, **43**, 1520–1525.
36 C. M. Leung, P. de Haan, K. Ronaldson-Bouchard, G.-A. Kim, J. Ko, H. S. Rho, Z. Chen, P. Habibovic, N. L. Jeon, S. Takayama, M. L. Shuler, G. Vunjak-Novakovic, O. Frey, E. Verpoorte and Y.-C. Toh, *Nat. Rev. Methods Primers*, 2022, **2**, 33.
37 C.-W. Chang, C.-C. Peng, W.-H. Liao and Y.-C. Tung, *Analyst*, 2015, **140**, 7355–7365.
38 R. Inaam, M. F. Bolontrade, S. Okamoto, T. Shibata, T. S. Santra and M. Nagai, *Micromachines*, 2025, **16**, 525.
39 I. Miranda, A. Souza, P. Sousa, J. Ribeiro, E. M. S. Castanheira, R. Lima and G. Minas, *J. Funct. Biomater.*, 2022, **13**, 2.
40 S.-u. Hassan, H. Morgan, X. Zhang and X. Niu, *Anal. Chem.*, 2015, **87**, 3895–3901.
41 I. Banerjee, T. Salih, H. Ramachandraiah, J. Erlandsson, T. Pettersson, A. C. Araújo, M. Karlsson and A. Russom, *RSC Adv.*, 2017, **7**, 35048–35054.
42 M. A. Catterton, A. G. Ball and R. R. Pompano, *Micromachines*, 2021, **12**, 993.
43 S. Begolo, D. V. Zhukov, D. A. Selck, L. Li and R. F. Ismagilov, *Lab Chip*, 2014, **14**, 4616–4628.
44 H. Liu, X. Li and R. M. Crooks, *Anal. Chem.*, 2013, **85**, 4263–4267.
45 X. Luan, Y. Pan, D. Zhou, B. He, X. Liu, Y. Gao, J. Yang and Y. Song, *Biosens. Bioelectron.*, 2020, **165**, 112406.
46 Y. Xia, Z. Liu, S. Yan, F. Yin, X. Feng and B.-F. Liu, *Sens. Actuators, B*, 2016, **228**, 491–499.
47 Y. Zhao, Z. Li, T. Li, R. Rao, J. Zhu, R. Hu, G. Xu, Y. Li and Y. Yang, *Anal. Chem.*, 2024, **96**, 20602–20611.
48 L. Tian, Y. Gao, Y. Lu, F. Xu, Z. Feng, L. Zi, Z. Deng and J. Yang, *Lab Chip*, 2025, **25**, 5762–5776.
49 J. E. Kreutz, T. Munson, T. Huynh, F. Shen, W. Du and R. F. Ismagilov, *Anal. Chem.*, 2011, **83**, 8158–8168.
50 F. Shen, B. Sun, J. E. Kreutz, E. K. Davydova, W. Du, P. L. Reddy, L. J. Joseph and R. F. Ismagilov, *J. Am. Chem. Soc.*, 2011, **133**, 17705–17712.
51 Y. Luo, Q. Hu, Y. Yu, W. Lyu and F. Shen, *Anal. Chim. Acta*, 2024, **1304**, 342541.
52 Q. Hu, F. Kanwal, W. Lyu, J. Zhang, X. Liu, K. Qin and F. Shen, *ACS Sens.*, 2023, **8**, 114–121.
53 Y. Yu, Z. Yu, X. Pan, L. Xu, R. Guo, X. Qian and F. Shen, *Analyst*, 2022, **147**, 625–633.
54 Y. Yu, S. Wang, Y. Luo, C. Gu, X. Shi and F. Shen, *ACS Sens.*, 2023, **8**, 3595–3603.
55 F. Shen, in *Microchip Diagnostics: Methods and Protocols*, ed. V. Taly, J.-L. Viovy and S. Descroix, Springer New York, New York, NY, 2017, pp. 123–132, DOI: 10.1007/978-1-4939-6734-6_10.
56 E. M. Khorosheva, M. A. Karymov, D. A. Selck and R. F. Ismagilov, *Nucleic Acids Res.*, 2016, **44**, e10.
57 B. Sun, F. Shen, S. E. McCalla, J. E. Kreutz, M. A. Karymov and R. F. Ismagilov, *Anal. Chem.*, 2013, **85**, 1540–1546.
58 D. A. Selck, M. A. Karymov, B. Sun and R. F. Ismagilov, *Anal. Chem.*, 2013, **85**, 11129–11136.
59 D. A. Selck and R. F. Ismagilov, *PLoS One*, 2016, **11**, e0163060.
60 N. G. Schoepp, T. S. Schlappi, M. S. Curtis, S. S. Butkovich, S. Miller, R. M. Humphries and R. F. Ismagilov, *Sci. Transl. Med.*, 2017, **9**, eaal3693.
61 J. Rodriguez-Manzano, M. A. Karymov, S. Begolo, D. A. Selck, D. V. Zhukov, E. Jue and R. F. Ismagilov, *ACS Nano*, 2016, **10**, 3102–3113.
62 L. Xu, H. Qu, D. G. Alonso, Z. Yu, Y. Yu, Y. Shi, C. Hu, T. Zhu, N. Wu and F. Shen, *Biosens. Bioelectron.*, 2021, **175**, 112908.
63 J. Zhang, L. Xu, Z. Sheng, J. Zheng, W. Chen, Q. Hu and F. Shen, *ACS Sens.*, 2024, **9**, 646–653.
64 J. Zhang, Z. Dong, L. Xu, X. Han, Z. Sheng, W. Chen, J. Zheng, D. Lai and F. Shen, *Adv. Sci.*, 2024, **11**, e2406367.
65 L. Xu, J. Jin, W. Lyu, X. Liang, Q. Wang, J. Zhang, Y. Luo, J. Chen, H. Lu, X. Li and F. Shen, *Biosens. Bioelectron.*, 2026, 118438, DOI: 10.1016/j.bios.2026.118438.
66 C. Xu, B. Ma, Z. Gao, X. Dong, C. Zhao and H. Liu, *Sci. Adv.*, 2021, **7**, eabk0100.
67 L. Li, W. Du and R. Ismagilov, *J. Am. Chem. Soc.*, 2010, **132**, 106–111.
68 L. Li and R. F. Ismagilov, *Annu. Rev. Biophys.*, 2010, **39**, 139–158.
69 W. Liu, D. Chen, W. Du, K. P. Nichols and R. F. Ismagilov, *Anal. Chem.*, 2010, **82**, 3276–3282.
70 Y. Song, Y. Zhang, P. E. Bernard, J. M. Reuben, N. T. Ueno, R. B. Arlinghaus, Y. Zu and L. Qin, *Nat. Commun.*, 2012, **3**, 1283.
71 M. S. Verma, M.-N. Tsaloglou, T. Sisley, D. Christodouleas, A. Chen, J. Milette and G. M. Whitesides, *Biosens. Bioelectron.*, 2018, **99**, 77–84.
72 S. E. Son, S. H. Cheon, W. Hur, H. B. Lee, D. H. Kim, C. H. Ha, S. J. Lee, D. K. Han and G. H. Seong, *Biosens. Bioelectron.*, 2024, **243**, 115752.
73 D. M. Rissin, C. W. Kan, T. G. Campbell, S. C. Howes, D. R. Fournier, L. Song, T. Piech, P. P. Patel, L. Chang, A. J. Rivnak, E. P. Ferrell, J. D. Randall, G. K. Provuncher, D. R. Walt and D. C. Duffy, *Nat. Biotechnol.*, 2010, **28**, 595–599.
74 S. Ge, W. Liu, T. Schlappi and R. F. Ismagilov, *J. Am. Chem. Soc.*, 2014, **136**, 14662–14665.
75 Y. Zhang, X. Li, J. Yi, W. Lyu, H. Wang, Q. Guo, T. Tang, F. Ou, H. Gu, F. Shen, Y. Wang and H. Xu, *ACS Sens.*, 2026, **11**, 74–85.
76 W. Lyu, X. Cheng, Z. Yu, R. Dong, Z. Sheng, T. Zhang, X. Yin and F. Shen, *Talanta*, 2024, **280**, 126782.
77 Y. Zhao, F. Pereira, A. J. deMello, H. Morgan and X. Niu, *Lab Chip*, 2014, **14**, 555–561.
78 S. Wang, S. Chen, J. Wang, P. Xu, Y. Luo, Z. Nie and W. Du, *Electrophoresis*, 2014, **35**, 2528–2533.

79 Q. Yi, D. Cai, M. Xiao, M. Nie, Q. Cui, J. Cheng, C. Li, J. Feng, G. Urban, Y.-C. Xu, Y. Lan and W. Du, *Biosens. Bioelectron.*, 2019, **135**, 200–207.
80 C. Wan, L. Yi, H. Yuan, S. Li, X. Wang, Y. Shu, H. Xie, M. Lei, Z. Miao, W. Du, X. Feng, Y. Li, P. Chen and B.-F. Liu, *Small Methods*, 2024, **8**, 2400454.
81 J. K.-H. Wat, M. Xu, L. Nan, H. Lin, K. K.-W. To, H. C. Shum and S. U. Hassan, *Microsyst. Nanoeng.*, 2025, **11**, 110.
82 G. Cai, W. Wu, S. Feng and Y. Liu, *Analyst*, 2021, **146**, 4622–4629.
83 L. Xue, M. Liao and J. Lin, *Lab Chip*, 2024, **24**, 4039–4049.
84 D. Chen, S.-J. Liu and W. Du, *J. Hazard. Mater.*, 2019, **366**, 512–519.
85 D. Cai, M. Xiao, P. Xu, Y.-C. Xu and W. Du, *Lab Chip*, 2014, **14**, 3917–3924.
86 X. Li, S. Wang, Z. Zhai, W. Wang, Y. Hao and J. Lin, *Food Control*, 2022, **140**, 109122.
87 Y. a. Ren, J. Qin, M. Li and F. Shen, *Anal. Chem.*, 2026, DOI: 10.1021/acs.analchem.5c07370.
88 L. Ma, S. S. Datta, M. A. Karymov, Q. Pan, S. Begolo and R. F. Ismagilov, *Integr. Biol.*, 2014, **6**, 796–805.
89 L. Ma, J. Kim, R. Hatzenpichler, M. A. Karymov, N. Hubert, I. M. Hanan, E. B. Chang and R. F. Ismagilov, *Proc. Natl. Acad. Sci. U. S. A.*, 2014, **111**, 9768–9773.
90 X. Li, Q. Hu, X. Liu, J. Liu, N. Wu and F. Shen, *Anal. Chem.*, 2023, **95**, 8632–8639.
91 M. A. Catterton, A. F. Dunn and R. R. Pompano, *Lab Chip*, 2018, **18**, 2003–2012.
92 F. Liu, J. Liu, Y. Luo, S. Wu, X. Liu, H. Chen, Z. Luo, H. Yuan, F. Shen, F. Zhu and J. Ye, *Adv. Sci.*, 2024, **11**, e2406668.
93 E. Iseri, K. Kaya, R. Heuchel and W. van der Wijngaart, *2022 IEEE 35th International Conference on Micro Electro Mechanical Systems Conference (MEMS)*, Tokyo, Japan, 2022, pp. 912–914.
94 H. Qu, M. Yu, W. Du, L. Xu, W. Lyu and F. Shen, *Langmuir*, 2020, **36**, 585–590.
95 J. Li, C. He, H. Qu, F. Shen and J. Ye, *J. Mater. Chem. C*, 2022, **10**, 7273–7282.
96 J. Li, F. Liu, C. He, F. Shen and J. Ye, *Nanophotonics*, 2022, **11**, 1549–1560.
97 M. N. Tsaloglou, R. J. Watson, C. M. Rushworth, Y. Zhao, X. Niu, J. M. Sutton and H. Morgan, *Analyst*, 2015, **140**, 258–264.
98 R. R. Pompano, W. Liu, W. Du and R. F. Ismagilov, *Annu. Rev. Anal. Chem.*, 2011, **4**, 59–81.
99 N. Venugopal Menon, J. Lee, T. Tang and C. T. Lim, *Lab Chip*, 2025, **25**, 752–763.
100 J. Zhou, J. Dong, H. Hou, L. Huang and J. Li, *Lab Chip*, 2024, **24**, 1307–1326.
101 Y. Wei, X. Liu, Y. Mu, C. Xu, G. Zhang, T. Li, Z. Li, W. Yuan, H.-P. Ho and M. Xu, *Biosens. Bioelectron.*, 2025, **288**, 117741.
102 S. Lian, X. Li and X. Lv, *ACS Appl. Mater. Interfaces*, 2025, **17**, 10193–10230.
103 S. T. Gebreyesus, A. A. Siyal, R. B. Kitata, E. S.-W. Chen, B. Enkhbayar, T. Angata, K.-I. Lin, Y.-J. Chen and H.-L. Tu, *Nat. Commun.*, 2022, **13**, 37.

